Center for Environmentally Sustainable Transportation in Cold Climates

# A Targeted Approach to High-Volume Fly Ash Concrete Pavement (Phase I)

**Sen Du**
**Xianming Shi**
**Department of Civil and Environmental Engineering**
**Washington State University**

**Date: December 2018**

**Prepared by: Sen Du and Xianming Shi**

Center for Environmentally Sustainable
Transportation in Cold Climates
University of Alaska Fairbanks
P.O. Box 755900
Fairbanks, AK 99775

U.S. Department of Transportation
1200 New Jersey Avenue, SE
Washington, DC 20590

**INE/CESTiCC 18.11**

# REPORT DOCUMENTATION PAGE

Form approved OMB No.



| 1. AGENCY USE ONLY (LEAVE BLANK) | 2. REPORT DATE | 3. REPORT TYPE AND DATES COVERED |
|---|---|---|
| | 06/2018 | Final Report: 11/2015 – 12/2018 |

4. TITLE AND SUBTITLE

A Targeted Approach to High-Volume Fly Ash Concrete Pavement (Phase I Report)

5. FUNDING NUMBERS

6. AUTHOR(S)

Sen Du, Washington State University
Xianming Shi, Ph.D., P.E., Washington State University

7. PERFORMING ORGANIZATION NAME(S) AND ADDRESS(ES)

Laboratory of Advanced & Sustainable Cementitious Materials
Washington State University
405 Spokane Street, Sloan 101, P.O. Box 755900
Pullman, WA 99164

8. PERFORMING ORGANIZATION REPORT NUMBER

INE/AUTC 18.11

9. SPONSORING/MONITORING AGENCY NAME(S) AND ADDRESS(ES)

U.S. Department of Transportation
1200 New Jersey Avenue, SE
Washington, DC 20590

10. SPONSORING/MONITORING AGENCY REPORT NUMBER

11. SUPPLENMENTARY NOTES

12a. DISTRIBUTION / AVAILABILITY STATEMENT

No restrictions

12b. DISTRIBUTION CODE

13. ABSTRACT (Maximum 200 words)

Unlike the conventional method of admixing nanomaterials directly in fresh concrete mixture, a more targeted approach was explored. Specifically, nanomaterials were used to improve the interface between coarse aggregate and cement paste, by coating the coarse aggregate with cement paste that contained graphene oxide or nanosilica. Using coated coarse aggregates, the mechanical and transport properties of high-volume fly ash (HVFA) concrete were tested to evaluate the effect of nanomaterial coating on the interface transition zone of concrete. The compressive and splitting strengths of HVFA concrete at 3, 7, 14, and 28 days and the water sorptivity and chloride migration coefficient at 28 days were studied. Results show that nanomaterial-coated coarse aggregate can improve the transport properties of HVFA concrete by reducing permeability. However, no improvement was seen in the compressive and splitting strengths when incorporating coated coarse aggregate, compared with direct mixing of nanomaterials in fresh concrete. Resistance to freezing/thawing cycles and scanning electron microscope/energy dispersive X-ray spectroscopy of concrete samples were also investigated to obtain a more comprehensive and mechanistic understanding of nanomaterial coating.

14- KEYWORDS:

High-volume fly ash, graphene oxide, nanosilica, coating, coarse aggregate

15. NUMBER OF PAGES

70

16. PRICE CODE

N/A

| 17. SECURITY CLASSIFICATION OF REPORT | 18. SECURITY CLASSIFICATION OF THIS PAGE | 19. SECURITY CLASSIFICATION OF ABSTRACT | 20. LIMITATION OF ABSTRACT |
|---|---|---|---|
| Unclassified | Unclassified | Unclassified | N/A |

# A Targeted Approach to High-Volume Fly Ash Concrete Pavement

# (Phase I Report)

**by**

**Sen Du**
**Xianming Shi, Ph.D., P.E.**

**Department of Civil and Environmental Engineering**
**Washington State University**
**Pullman, WA 99164**

**INE/AUTC 18.11**

**December 2018**

**DISCLAIMER**

This document is disseminated under the sponsorship of the U.S. Department of Transportation in the interest of information exchange. The U.S. Government assumes no liability for the use of the information contained in this document. The U.S. Government does not endorse products or manufacturers. Trademarks or manufacturer names appear in this report only because they are considered essential to the objective of the document.

Opinions and conclusions expressed or implied in the report are those of the authors. They are not necessarily those of the funding agencies.

# METRIC (SI*) CONVERSION FACTORS

## APPROXIMATE CONVERSIONS TO SI UNITS

| Symbol | When You Know | Multiply By | To Find | Symbol |
|---|---|---|---|---|
| | | LENGTH | | |
| in | inches | 25.4 | millimeters | mm |
| ft | feet | 0.3048 | meters | m |
| yd | yards | 0.914 | meters | m |
| mi | Miles (statute) | 1.61 | kilometers | km |
| | | AREA | | |
| $in^2$ | square inches | 645.2 | millimeters squared | |
| | $cm^2$ $ft^2$ | square feet | 0.0929 | |
| | meters squared | $m^2$ | | |
| $yd^2$ | square yards | 0.836 | meters squared | $m^2$ |
| $mi^2$ | square miles | 2.59 | kilometers squared | $km^2$ |
| ac | acres | 0.4046 | hectares | ha |
| | | MASS (weight) | | |
| oz | Ounces (avdp) | 28.35 | grams | g |
| lb | Pounds (avdp) | 0.454 | kilograms | kg |
| T | Short tons (2000 lb) | 0.907 | megagrams | mg |
| | | VOLUME | | |
| fl oz | fluid ounces (US) | 29.57 | milliliters | mL |
| gal | Gallons (liq) | 3.785 | liters | liters |
| $ft^3$ | cubic feet | 0.0283 | meters cubed | $m^3$ |
| $yd^3$ | cubic yards | 0.765 | meters cubed | $m^3$ |

Note: Volumes greater than 1000 L shall be shown in $m^3$

| | | | | |
|---|---|---|---|---|
| | | TEMPERATURE (exact) | | |
| $^oF$ | Fahrenheit | 5/9 ($^oF$-32) | Celsius | |
| | | $^oC$ temperature | temperature | |
| | | ILLUMINATION | | |
| fc | Foot-candles | 10.76 | lux | lx |
| fl | foot-lamberts | 3.426 | candela/$m^2$ | $cd/cm^2$ |
| | | FORCE and PRESSURE or STRESS | | |
| lbf | pound-force | 4.45 | newtons | N |
| psi | pound-force per square inch | 6.89 | kilopascals | kPa |

These factors conform to the requirement of FHWA Order 5190.1A *SI is the symbol for the International System of Measurements

## APPROXIMATE CONVERSIONS FROM SI UNITS

| Symbol | When You Know | Multiply By | To Find | Symbol |
|---|---|---|---|---|
| | | LENGTH | | |
| mm | millimeters | 0.039 | inches | in |
| m | meters | 3.28 | feet | ft |
| m | meters | 1.09 | yards | yd |
| km | kilometers | 0.621 | Miles (statute) | mi |
| | | AREA | | |
| $mm^2$ | millimeters squared | 0.0016 | square inches | $in^2$ |
| $m^2$ | meters squared | 10.764 | square feet | $ft^2$ |
| $km^2$ | kilometers squared | 0.39 | square miles | $mi^2$ |
| ha | hectares (10,000 $m^2$) | 2.471 | acres | ac |
| | | MASS (weight) | | |
| g | grams | 0.0353 | Ounces (avdp) | oz |
| kg | kilograms | 2.205 | Pounds (avdp) | lb |
| mg | megagrams (1000 kg) | 1.103 | short tons | T |
| | | VOLUME | | |
| mL | milliliters | 0.034 | fluid ounces (US) | fl oz |
| liters | liters | 0.264 | Gallons (liq) | gal |
| $m^3$ | meters cubed | 35.315 | cubic feet | $ft^3$ |
| $m^3$ | meters cubed | 1.308 | cubic yards | $yd^3$ |
| | | TEMPERATURE (exact) | | |
| $^oC$ | Celsius temperature | 9/5 $^oC$+32 | Fahrenheit temperature | $^oF$ |
| | | ILLUMINATION | | |
| lx | lux | 0.0929 | foot-candles | fc |
| cd/cm 2 | candela/$m^2$ | 0.2919 | foot-lamberts | fl |
| | | FORCE and PRESSURE or STRESS | | |
| N | newtons | 0.225 | pound-force | lbf |
| kPa | kilopascals | 0.145 | pound-force per square inch | psi |

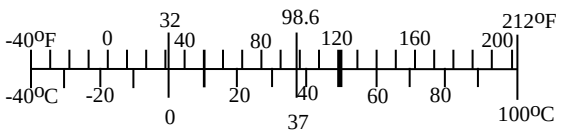

**ACKNOWLEDGMENTS**

The authors would like to thank the Center for Environmentally Sustainable Transportation in Cold Climates (CESTiCC) for funding this work. The authors would also like to thank Dr. Scott Boroughs at the WSU Peter Hooper GeoAnalytical Lab for his assistance in the use of the microprobe.

**TABLE OF CONTENTS**

## LIST OF FIGURES

## LIST OF TABLES

## EXECUTIVE SUMMARY

The primary objective of this project during Phase I was to develop a viable method of using nanotechnology in treating coarse aggregate (or coal fly ash) before its use in sustainable fly ash concrete pavement. The application of nanotechnology to address weak interfaces in this type of sustainable concrete is a highly innovative idea. After extensive trials, coating coarse aggregate with cement paste containing graphene oxide or nanosilica was selected as the best approach in the investigation of the mechanical and transport properties of concrete. Results of the mechanical properties tests showed that high-volume fly ash (HVFA) concrete exhibited 28-day compressive and splitting strengths similar to ordinary Portland cement concrete. The use of coated coarse aggregate showed no significant benefit compared with direct mixing of nanomaterial in fresh concrete. As expected, HVFA concrete showed faster strength development at the late curing time (from 14 to 28 days), starting with relatively low early-age strength. Incorporating coated coarse aggregate in HVFA concrete resulted in a reduced water sorptivity and chloride migration coefficient. These improved transport properties were attributed mainly to the improved interfacial transition zone (ITZ) in HVFA concrete.

To obtain more information on the effect of nanomaterial coating on the concrete ITZ, freezing/thawing cycle tests and scanning electron microscope/energy dispersive X-ray spectroscopy characterization were conducted on selected concrete samples. Results indicate a relationship between the transport properties and freezing/thawing resistance of concrete. Microstructure images, element content, and element ratios in both the ITZ and paste matrix provided deeper understanding of the performance of HVFA concrete at multiple scales.

# CHAPTER 1 INTRODUCTION

## 1.1 Background

An increased proportion of fly ash to replace cement in concrete mixtures can make concrete a more sustainable and environmentally friendly material [1], assuming there is no significant sacrifice in the product's performance and durability. Fly ash is the main by-product of coal combustion in electrical energy production. In 2012, the global annual generation of fly ash was approximately 750 million tons [2], yet only about 25% of fly ash was recycled or reutilized [3]. By 2015, a more up-to-date and detailed estimate of the generation and utilization rates of fly ash in China and the U.S. was 580 million tons and nearly 30%, and 130 million tons and approximately 50%, respectively [4]. In addition to its use as a soil amendment, in road base construction, and as filler in polymers, fly ash could have increasing utilization in concrete [5]. A low utilization rate of fly ash means that this material may end up in landfills and result in significant water and soil pollution; heavy metal contamination is of particular environmental concern [4].

Using fly ash in concrete or mortar is an effective way to solidify its potential hazardous elements, as well as an economical way to improve some of the properties of concrete or mortar. Traditionally, the amount of fly ash replacement of cement has been limited by specification to 20–25% by mass due to concerns over loss in concrete's early-age strength and resistance to freeze/thaw and salt scaling [6], [7]. High-volume fly ash (HVFA) concrete is defined as concrete in which the replacement of cement by fly ash is at least 50% [8]. This type of concrete was first successfully used in structural projects in the late 1980s by the Canadian Center for Mineral and Energy Technology (CANMET) [9]. With a water-to-binder ratio typically of 0.3 or

lower, HVFA concrete was reported to have many advantages, such as acceptable early-age strength, high long-term strength, low drying shrinkage, and durability performance comparable to or better than Portland cement concrete at the same strength [10].

The application of nanomaterials in concrete is probably one of the best ways to tackle the inherent issues of HVFA concrete. It is well known that the behavior of concrete materials depends largely on cement hydration products, mainly calcium silicate hydrates (C-S-H), whose size lies in the nanometer range. Understanding the characteristics of hydration products at the nanoscale should facilitate the efficient manipulation of microstructure and chemistry of HVFA concrete [11]. Nanotechnology has demonstrated clear benefits in empowering the development of concrete with enhanced durability and mechanical properties [12], [13]. With increased usage and production over the last two decades, the cost of non-toxic user-friendly nanomaterials (e.g., nanoclays, nanosilica, and nano-$CaCO_3$) has dropped exponentially, and this trend is expected to continue.

## 1.2 Problem Statement

The wider use of fly ash in concrete is hindered by performance concerns and lack of understanding of such sustainable concrete at microscopic and higher levels [14]–[18]. For instance, the potential incompatibilities between fly ash, cement, and admixtures remain poorly understood, as do the sequence of chemical reactions underlying the strength and microstructure development of such unconventional concretes. There are many recently published studies related to the use of nano-/micro-modification to alter the surface properties of various materials [19], [20] or to enhance the bulk properties of concrete materials [21], [22]. It was found that nanotechnology can bring fundamental changes to unconventional and environmentally friendly concretes by enhancing their processing, mechanical, and durability properties with a “bottom-

up" approach. Recent advances in nanotechnology may provide tools that shed more light on the aggregate-paste interface in sustainable concrete and address the inherent weakness of the interfacial transition zone (ITZ) that represents a thin-shell region (typically 10 to 50 microns thick) surrounding coarse aggregate particles. Nanoscience and nanoengineering may also be employed to enhance the weak interface between a fly ash particle and its surrounding paste.

Research is needed to advance the understanding of using nanotechnology for HVFA concrete, especially when such concrete is intended for pavement applications.

## 1.3 Scope of Work

To achieve the project objectives, this study was designed to include the following tasks:

1. Preparation and characterization of materials: This task involved the selection of nanoscale treatment methods for fly ash and coarse aggregate.
2. Laboratory evaluation of the selected nanoscale surface treatment methods for fly ash and coarse aggregate: This task involved the identification and evaluation of the appropriate nanoscale surface treatment methods on selected fly ash and coarse aggregate, with a focus on selected HVFA concrete mixes.
3. Micron and submicron understanding: In this task, scanning electron microscope (SEM)/energy dispersive X-ray spectroscopy (EDS) was employed to characterize both the sustainable concrete and the control specimens.

## 1.4 Outline of Report

Chapter 2 presents the procedure and results of selecting the appropriate nanoscale surface treatment method for both fly ash and coarse aggregate. Chapter 3 provides the laboratory evaluation of HVFA concrete containing nanomaterial-treated fly ash or coarse

aggregate, and includes a discussion of the microstructure investigation of the ITZ of HVFA concrete. Chapter 4 summarizes the key findings of this work.

# CHAPTER 2 NANOMATERIALS TREATMENT METHOD SELECTION

## 2.1 Introduction

The use of nanomaterials in concrete to enhance its properties and/or performance has received considerable attention. The admixed nanomaterials in concrete work mainly in two ways: (1) as superb filler and (2) in cement hydration [23], [24]. While nanomaterials may cause deficiencies in some properties of concrete, such as in workability due to high water demand, their beneficial effect on concrete's technical properties has been demonstrated clearly [24]. The most commonly used nanomaterials are nanoscale spherical materials (nano-$SiO_2$, $TiO_2$, $Al_2O_3$, $Fe_2O_3$, etc.), nanotubes and fibers (carbon nanotubes and carbon nanofibers), and nanoplatelets (nanoclays, graphene, and graphite oxide) [25]–[27]. The incorporation of these nanomaterials in concrete can impart advanced properties required for concrete construction, such as improved mechanical properties, compactness, and durability [28], [29].

Nanotechnology can focus on the development of nanobinders or nanoengineered cement-based materials through the "bottom-up" approach [30]–[32]. "Bottom-up" engineering, spanning atomic or nanoscale to mesoscopic and macroscopic scales, aims to alter the bulk properties of material, from engineering modification to molecular structure [33], [34]. Among chemical technologies, sol-gel synthesis is one of the widely used "bottom-up" production methods for nanomaterials [35].

Nanomodification that focuses on key interfaces instead of the bulk matrix of concrete remains underexplored. This approach could significantly reduce the cost of nanomodification while addressing the root cause of concrete failures. Similar nanomodification has proven effective in greatly improving the ITZ structure and overall performance of mortar and concrete

[36], [37]. Generally, nanomodification on key interfaces includes nanoscale surface treatment through dip-coating in solutions of nanoparticles and aqueous nanofilm growth on the surface of fly ash particles or coarse aggregate. In the dip-coat method, an aqueous solution with exfoliated nanoparticles is used to dip-coat fly ash or coarse aggregate under mechanical stirring. In the aqueous nanofilm growth method, nanofilm could be in situ chemically grown on the surface of interest by using the fly ash or coarse aggregate silica phase as the substrate [38]–[40].

This chapter evaluates the effect of surface treatment using various nanomaterials on fly ash particles and coarse aggregate. Both dip-coat and aqueous nanofilm growth methods were explored to treat fly ash particles or coarse aggregate. Furthermore, early-age compressive strength, water sorptivity, or gas permeability of the corresponding HVFA mortar or concrete samples was tested for selecting the appropriate treatment method.

## 2.2 Experimental Program

### 2.2.1 Materials

High-volume fly ash mortars were used to investigate the effect of nanomaterial surface treatment on fly ash particles. The HVFA mortar consisted of ASTM Type I/II Portland cement and fly ash as binder. Two types of fly ash were obtained from coal-fired power plants in the western United States: one type of Class C fly ash and one type of Class F fly ash. The chemical composition of fly ash is mainly $SiO_2$, $Al_2O_3$, $Fe_2O_3$, CaO, and MgO. According to ASTM C618, Class C fly ash features a total content of $SiO_2$, $Al_2O_3$, and $Fe_2O_3$ greater than 50% and CaO content of 20% or higher, whereas Class F fly ash features a total content of $SiO_2$, $Al_2O_3$, and $Fe_2O_3$ greater than 70% and a lower CaO content. In general, Class F fly ash exhibits pozzolanic properties, whereas Class C fly ash exhibits pozzolanic and cementitious properties simultaneously, and these characteristics make fly ash a likely beneficial supplementary

cementitious material (SCM) [41]. The chemical composition of ordinary Portland cement (OPC) and fly ash is provided in Table 2.1. The particle size distribution of OPC and Class C fly ash was measured using a laser scattering particle-size distribution analyzer. Figure 2.1 shows the particle size distribution of OPC and fly ash. It can be seen in this figure that fly ash particles are finer than OPC particles.

The fine aggregate was natural sand with a nominal maximum size of 4.75 mm and a fineness modulus of 2.7. The coarse aggregate was 19 mm nominal maximum-size crushed limestone. Both aggregates met the requirements of ASTM C33 and were used in surface saturated dry (SSD) condition. The results of sieve analysis of both aggregates are presented in Figure 2.2. The high-range water-reducing agent (HRWRA) used was a polycarboxylic-ether type superplasticizer with a specific gravity of 1.08, pH of 5.0, and solid content of 34.4%.

**Table 2.1** Chemical composition of cement and fly ash

| **Chemical Composition (wt.%)** | **OPC** | **Class C Fly Ash** | **Class F Fly Ash** |
|---|---|---|---|
| $Al_2O_3$ | 3.97 | 18.35 | 16.82 |
| $SiO_2$ | 20.44 | 32.52 | 49.81 |
| $Fe_2O_3$ | 4.07 | 4.80 | 5.72 |
| CaO | 62.90 | 28.38 | 13.9 |
| MgO | 2.42 | 5.33 | 4.19 |
| $Na_2O$ | 0.37 | 6.11 | 3.5 |
| $K_2O$ | 0.43 | 0.41 | 1.72 |
| $SO_3$ | 2.6 | 1.03 | 2.27 |
| LOI* | 2.7 | 1.5 | 1.07 |

* Loss on ignition

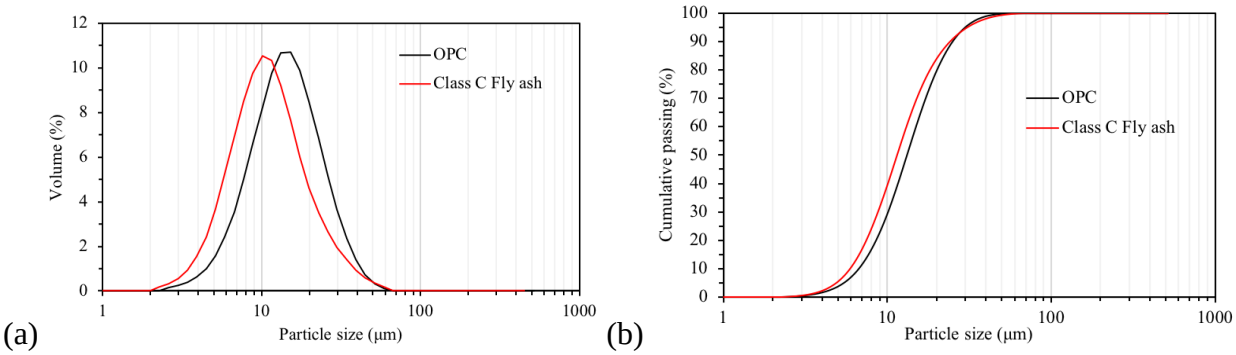


**Figure 2.1** Particle size distribution of OPC and Class C fly ash: (a) volume at each size and (b) cumulative passing

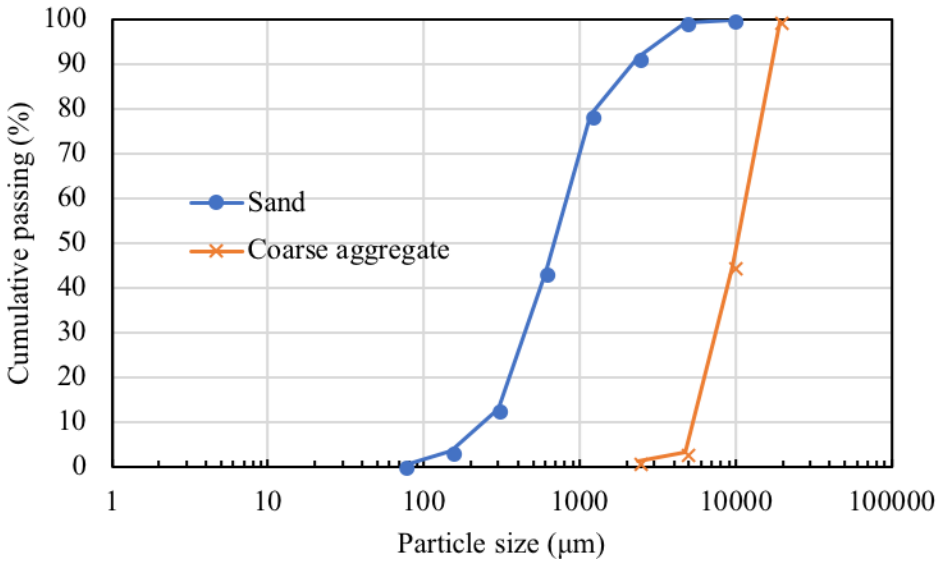


**Figure 2.2** Particle size distribution of sand and coarse aggregate

### 2.2.2 Surface treatment methods and mixing proportions

Both the dip-coat in solutions of nanoparticles and the aqueous nanofilm growth on fly ash particle or coarse aggregate surfaces were explored. The nanomaterials used included graphene oxide (GO), nanosilica (NS), nanoclay (NC), nano-$CaCO_3$ (NCa), cellulose nanofiber (CNF), cellulose nanocrystal (CNC), nano-$Al_2O_3$ (NA), and nanomontmorillonoid (NM). The aqueous solutions used for nanofilm growth included NaOH, the mixture of $Mg(Cl)_2$ and NaOH, and the mixture of $Ca(Cl)_2$ and NaOH. The nanomaterials were selected based on their reported

benefits in improving the strength and durability of concrete at an appropriate dosage [42]–[47]. The alkali solutions were used in light of the previous research that succeeded in forming C-S-H with the help of $SiO_2$ [48], which is a main composition of fly ash.

In order to select the best surface treatment method for the fly ash particles or coarse aggregate, three trials were conducted. In the first trial, GO and NC suspensions were used to coat fly ash particles in a filter bag (Figure 2.3). The GO or NC suspension was prepared using mixing water and the appropriate dosage of GO or NC, which made the concentration of GO and NC suspension 1g/L and 10g/L, respectively. The mesh size of the filter bag was smaller than the fly ash particles, which stopped them from fleeing the bag into suspension, yet at the same time was large enough for the nanomaterials (in this trial, GO and NC) from the suspension to pass through the bag to coat the fly ash particles. To prevent the bag from absorbing water from the nanomaterial suspension, the bag was pre-wetted by the corresponding suspension.


**Figure 2.3** Fly ash in filter bag soaking in GO suspension

The fly ash particles in the filter bag were treated for different lengths of time, ranging from 1 minute to 2 hours, beyond which the fly ash mud would become too hard to mix with other ingredients. After dip-coating in the nanomaterial suspension, the filter bag was lifted from the suspension and dried for 5 minutes to allow the extra water to drip back into the suspension, as shown in Figure 2.4. Then the remaining suspension was mixed with the fly ash mud and sand in a mortar mixer for 5 minutes according to the mixing proportions shown in Table 2.2. The NaOH solution was also used to treat fly ash particles using the same procedure, except that the nanomaterial suspension was changed to 0.1 mol/L NaOH solution. In Table 2.2, Control is the HVFA mortar made only with cement, fly ash, water, and sand. Coating Material-Control, for example, GO-Control, is the HVFA mortar that mixed GO suspension directly with cement, fly ash, and sand. Coating Material-Time stands for treating the fly ash particles for the specific time before mixing them with the remaining ingredients.

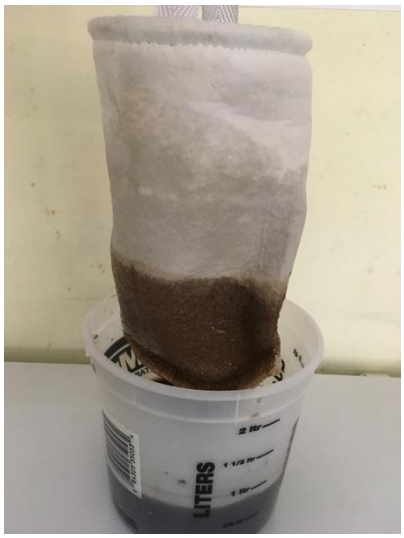


**Figure 2.4** Filter bag hanging on the container of the GO suspension after dip-coating

**Table 2.2** Mixing proportions for the designed HVFA mortars in Trial 1

| Mix | Cement ($kg/m^3$) | Fly ash ($kg/m^3$) | Water ($kg/m^3$) | Sand ($kg/m^3$) | Coating Materials ($g/m^3$) |
|---|---|---|---|---|---|

| | | | | | |
|---|---|---|---|---|---|
| Control | 180 | 270 | 135 | 675 | - |
| GO-Control | 180 | 270 | 135 | 675 | GO, 135 |
| GO-Time | 180 | 270 | 135 | 675 | GO, 135 |
| NC-Control | 180 | 270 | 135 | 675 | NC, 1350 |
| NC-Time | 180 | 270 | 135 | 675 | NC, 1350 |
| NaOH-Control | 180 | 270 | 135 | 675 | NaOH, 540 |
| NaOH-Time | 180 | 270 | 135 | 675 | NaOH, 540 |

The total amount of binder was kept at 450 kg/m$^3$, while the replacement of cement by fly ash was 60%. The sand-to-binder mass ratio was set at 1.5:1 to achieve a reasonably workable and homogeneous mixture with the help of the proper dosage of HRWRA. In the mixing process, HRWRA was admixed into each designed mortar at the appropriate dosage to achieve desirable workability (as a self-consolidating mortar). By using a mini slump cone test apparatus (with a base diameter of 100 mm, a top diameter of 70 mm and a height of 60 mm), the fresh HVFA mortars achieved outstanding flowability, with the spread diameter ranging from 180 mm to 220 mm. After mixing, fresh mortar was cast into 51 mm (diameter) × 102 mm (height) cylinder molds, which were covered with plastic membrane and left at room temperature for 24 hours. The HVFA mortars were then demolded and cured in a wet chamber (temperature: 22° ± 2°C, relative humidity: 98%) for an additional 6 or 27 days before further testing.

In the second trial, more types of nanomaterials were chosen to investigate their effects on the 3-day compressive strength of HVFA mortars, including NS, NCa, CNF, CNC, NA, NM, the mixture of $Mg(Cl)_2$ and NaOH, and the mixture of $Ca(Cl)_2$ and NaOH. Mixing proportions of each designed HVFA mortar are shown in

Table **2.3**. The mix that performed best in the compressive strength of HVFA mortar was used to coat fly ash particles in the next step, using the same procedure as that used in the first trial.

**Table 2.3** Mixing proportions for the designed HVFA mortars in Trial 2

| Mix | Cement ($kg/m^3$) | Fly ash ($kg/m^3$) | Water ($kg/m^3$) | Sand ($kg/m^3$) | Adding Materials |
|---|---|---|---|---|---|
| Control | 180 | 270 | 135 | 675 | - |
| 5% NS | 180 | 270 | 135 | 675 | NS, 22.5 $kg/m^3$ |
| 5% NCa | 180 | 270 | 135 | 675 | NCa, 22.5 $kg/m^3$ |
| 0.5% CNF | 180 | 270 | 135 | 675 | CNF, 2.25 $kg/m^3$ |
| 0.1% CNC | 180 | 270 | 135 | 675 | CNC, 0.45 $kg/m^3$ |
| 1% NA | 180 | 270 | 135 | 675 | NA, 4.5 $kg/m^3$ |
| 0.5% NM | 180 | 270 | 135 | 675 | NM, 2.25 $kg/m^3$ |
| $Mg(Cl)_2$+NaOH | 180 | 270 | 135 | 675 | $Mg(Cl)_2$+NaOH, 0.1 mol/L+0.2 mol/L |
| $Ca(Cl)_2$+NaOH | 180 | 270 | 135 | 675 | $Ca(Cl)_2$+NaOH, 0.1 mol/L+0.2 mol/L |

In the third trial, coarse aggregate was coated with cement pastes containing different nanomaterials, aimed at improving the interfacial transition zone (ITZ) of HVFA concrete, thus enhancing its transport and freezing/thawing performance. For this purpose, HVFA concrete samples with four different proportion designs were cast, as detailed in Table 2.4. In the last three groups, the variable is the paste used to coat coarse aggregate. The mixing proportions are shown in Table 2.5. The adopted three types of nanomaterials in this trial were GO, NS, and NC, with an incorporation level of 0.1%, 1%, and 0.5%, respectively, by weight of the cement. For the coating pastes, sufficient superplasticizer was used to make the paste flowable, ensuring only a thin paste film (typically less than 0.5 mm) on each coarse aggregate (Figure 2.5). Following about 4 hours of curing, the coated coarse aggregate was cast together with other materials to produce HVFA concrete samples. After being mixed, the fresh concrete was cast into 101.6 mm (diameter) × 203.2 mm (height) cylinder molds for compressive strength or chloride migration tests at the curing time of 7 or 28 days.

**Table 2.4** Mixing proportions for the designed HVFA concrete in Trial 3

| Mix | Cement ($kg/m^3$) | Class C Fly Ash ($kg/m^3$) | Water ($kg/m^3$) | W/B | Fine Aggregate ($kg/m^3$) | Coarse Aggregate ($kg/m^3$) |
|---|---|---|---|---|---|---|
| Control | 200 | 300 | 150 | 0.3 | 750 | 750 |
| GO Paste | 200 | 300 | 150 | 0.3 | 750 | 750 |
| NS Paste | 200 | 300 | 150 | 0.3 | 750 | 750 |
| NC Paste | 200 | 300 | 150 | 0.3 | 750 | 750 |

**Table 2.5** Mixing design for coating cement pastes

| Paste | Cement ($kg/m^3$) | Water ($kg/m^3$) | W/C | Adding Nanomaterials ($kg/m_3$) |
|---|---|---|---|---|
| Control | 500 | 125 | 0.25 | - |
| GO Paste | 500 | 125 | 0.25 | GO, 0.5 |
| NS Paste | 500 | 125 | 0.25 | NS, 5 |
| NC Paste | 500 | 125 | 0.25 | NC, 2.5 |

(a)  (b) 

**Figure 2.5** Coarse aggregate coated by cement paste:
(a) fresh state and (b) after 4 hours of curing

### 2.2.3 Test methods

Compressive strength was tested at curing for 28 days using a SATEC compression test machine by following ASTM C109.

The water sorptivity test was employed to determine the rate of water absorption in mortars, which primarily depends on porosity in the paste [49], [50]. The specimens used were 10 mm thick slices, cut from the middle part of cylinder mortar samples. After being cut, the disk specimens were oven-dried at 60°C in a condition of vacuum of 84.6 kPa (25 inHg) for 24 hours to remove any moisture inside them. Note that a vacuum of 25 inHg corresponds to the boiling point of water at about 56°C. Once the disk specimens cooled to room temperature, the top surface of each was covered with plastic wrap, and the side surface was sealed using tape to make sure that only the bottom surface was in contact with water during the test. Moisture rise in specimens was measured by recording the weight of specimens at regular time intervals. The sorptivity coefficient $k$ (mm/s$^{1/2}$) examined herein was the initial rate of absorption (in the first 6 hours) and can be calculated using the following equation according to ASTM C1585:

$$I = \frac{m_t}{a \times d} = k\sqrt{t} \quad (1)$$

where $I$ is the absorption, $m_t$ is the change in specimen mass (g) at the time $t$, $a$ is the exposed area of the specimen (mm$^2$), $d$ is the density of water in g/mm$^3$, and $t$ is the time (s).

In the gas permeability test, liquid methanol was used as the gas source to determine the gas transport properties of the HVFA mortars. Similar to the water sorptivity test, before testing occurred, 10 mm disk specimens were cut and oven-dried for 24 hours at a temperature of 60°C and a vacuum of 84.6 kPa (25 inHg). Subsequently, some methanol liquid was added to a cell, and the specimen was placed on top of the cell (with a rubber O-ring) and fixed by screws to avoid any leakage of methanol vapor, as shown in Figure 2.6. At the beginning of the test, the whole setup including the cell, specimen, and methanol was measured to obtain the initial weight. Then the whole setup was put in a water bath, with the temperature kept constant at 40°C and the water level always kept higher than the methanol liquid level in the cell. The

measurement of mass loss versus time due to vaporization of methanol liquid was recorded at each time interval until a steady-state mass loss was reached. The gas permeability coefficient $k_g$ ($m^2/s$) can be calculated using the following equations according to Darcy's law [51]:

$$P_v = 10^{\left(8.0809-\frac{1582.2}{239.76+T}\right)} \tag{2}$$

$$\eta = 10^{-7}\left(4.7169T^{0.618} - 99e^{-8.7593\times10^{-4}T} + 94e^{-7.916\times10^{-3}T} + 5\right) \tag{3}$$

$$Q = \frac{266\times10^{-3}m\prime}{10^{\left(8.0809-\frac{1582.2}{239.76+T}\right)}}T \tag{4}$$

$$k_g = \frac{2L\eta P_2 Q}{A\left(P_1^2-P_2^2\right)} \tag{5}$$

where $P_v$ is the absolute pressure of vapor ($N/m^2$), $T$ is the absolute temperature (K), η is dynamic viscosity ($N/m^2$), $Q$ is the volumetric flow rate ($m^3/s$), $m'$ is the rate of mass loss (g/s), $P_1$ is the inlet pressure ($N/m^2$), $P_2$ is the outlet pressure ($N/m^2$), $L$ is the thickness of the sample (m), and $A$ is the cross-sectional area perpendicular to the flow direction ($m^2$).

(a)  (b) 

**Figure 2.6** Experimental setup for gas permeability test

The chloride migration coefficient of concrete was investigated by using the rapid chloride migration (RCM) test, described in the guideline NT Build 492. The specimens used were 50 mm thick slices cut from the middle part of the concrete cylinders (two specimens from each cylinder). After being cut, the disk specimens were saturated with limewater under vacuum conditions 1 day prior to the RCM test, which was performed on the saturated concrete samples at the age of 28 days. The scheme of the RCM test setup is shown in Figure 2.7. A power supply with constant voltage output was used to connect the cathode and the anode. The catholyte and anolyte used were 10% NaCl solution and 0.3 M NaOH solution, respectively. The electrolytes were refreshed after each test. After the migration test (which generally takes 24 hours, depending on the applied voltage), the concrete samples were split and sprayed with a 0.1 M $AgNO_3$ solution to measure the penetration depth of chloride. Then the chloride migration coefficient $D_{RCM}$ was obtained using Eq. (6):

$$D_{RCM} = \frac{0.0239(273+T)L}{(U-2)t}\left(x_d - 0.0238\sqrt{\frac{(273+T)Lx_d}{U-2}}\right) \quad (6)$$

where $T$ is the average value of the initial and final temperatures in the solution (°C), $L$ is the thickness of the specimen (mm), $U$ is the applied voltage (V), $t$ is the duration of the test (h), and $x_d$ is the chloride penetration depth (mm).

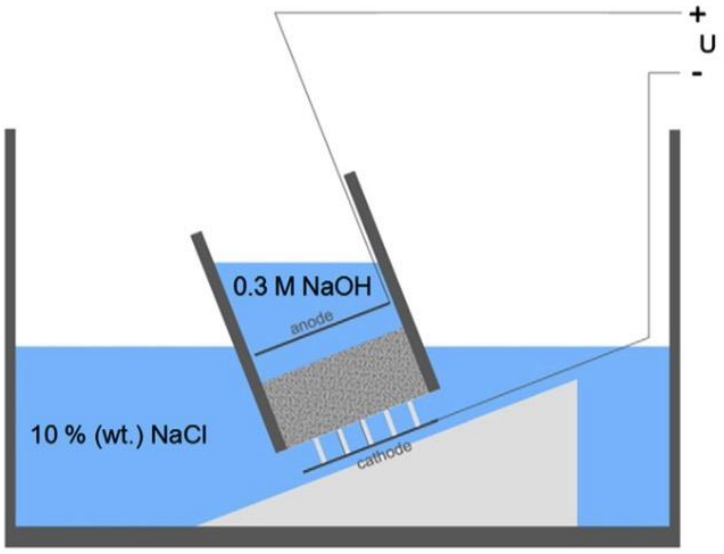


**Figure 2.7** The arrangement of the migration setup [52]

## 2.3 Results and Discussion

### 2.3.1 Surface treatment of fly ash in Trial 1

In the first trial, Class F fly ash was used to investigate the effect of nanomaterial surface treatment on the compressive strength of HVFA mortars. Figure 2.8,

Figure **2.9**, and Figure 2.10 present the 7-day compressive strength of HVFA mortars containing fly ash particles coated by GO suspension, NC suspension, and NaOH solution, respectively. It was clear that GO-2h and NC-30min were the two mixtures that performed best when compared with control mixtures, GO-Control and NC-Control, respectively. However, when treating fly ash particles in NaOH solution using the aqueous nanofilm growth method, no improvement was found in early-age compressive strength. This result indicates that more than 1 hour is needed to break the glass structure of fly ash under high alkalinity [53]. It was interesting to find that the early-age compressive strength of mixtures GO-Control and NC-Control was lower than their control counterparts. One reason may be the low activation and hydration degree of fly ash in early age, at which stage the fly ash mainly acts as micro aggregate in HVFA

mortars [54]. The adverse effect of the incorporation of nanomaterials on the early-age compressive strength of HVFA mortars needs further investigation. In fact, this effect was only found in the HVFA mortar produced with Class F fly ash.

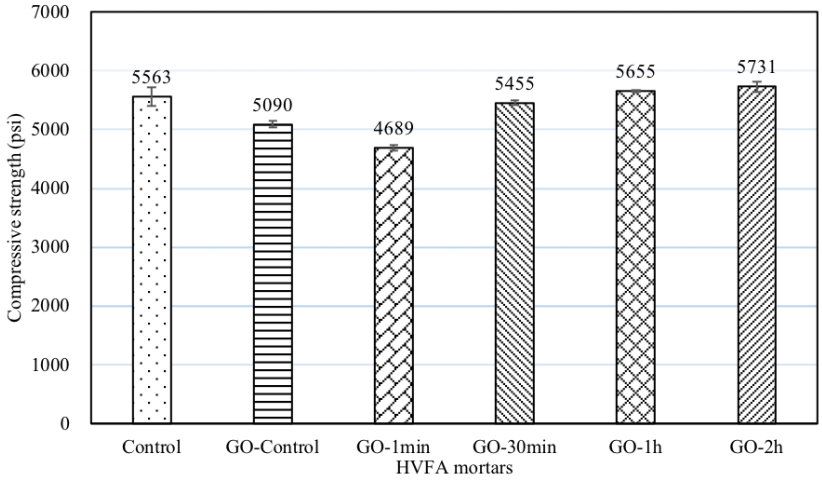


**Figure 2.8** 7-day compressive strength of HVFA mortars containing fly ash coated by GO

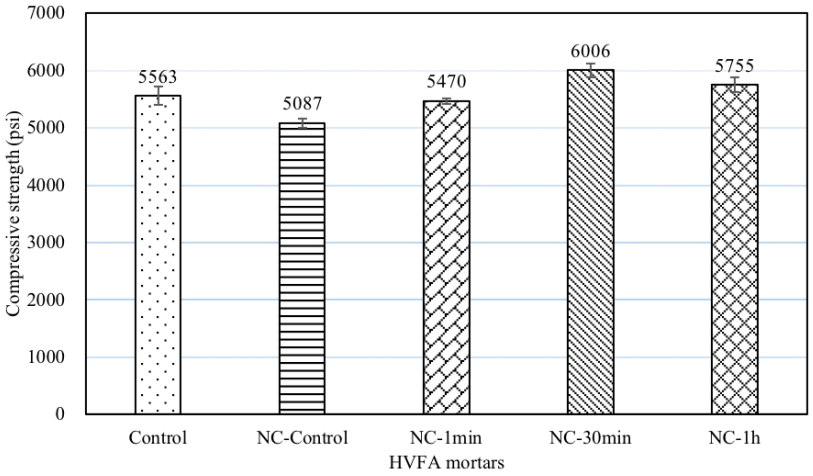


**Figure 2.9** 7-day compressive strength of HVFA mortars containing fly ash coated by NC

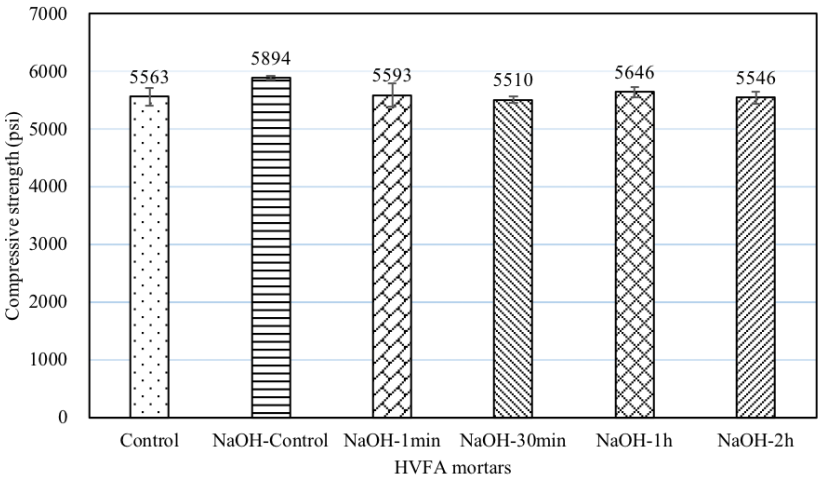


**Figure 2.10** 7-day compressive strength of HVFA mortars containing fly ash coated by NaOH

For the 28-day compressive strength test, mixtures GO-2h, NC-30min, and NaOH-1h were selected, since they performed best in the 7-day compressive strength test of HVFA mortars that contained coated fly ash particles. There was some, but not significant, increase in the 28-day compressive strength when compared with mixtures of directly mixed nanomaterials with other ingredients: 3.25%, 7.65%, and 9.63%, respectively, as shown in Figure 2.11, Figure 2.12, and Figure 2.13. Note that mixture NaOH-1h also exhibited improved 28-day compressive strength, which facilitates the activation of fly ash by alkali at late age. Furthermore, all HVFA

mortars showed significant evolution in compressive strength development from 7 days to 28 days, increasing from ~5000 psi to ~8000 psi.

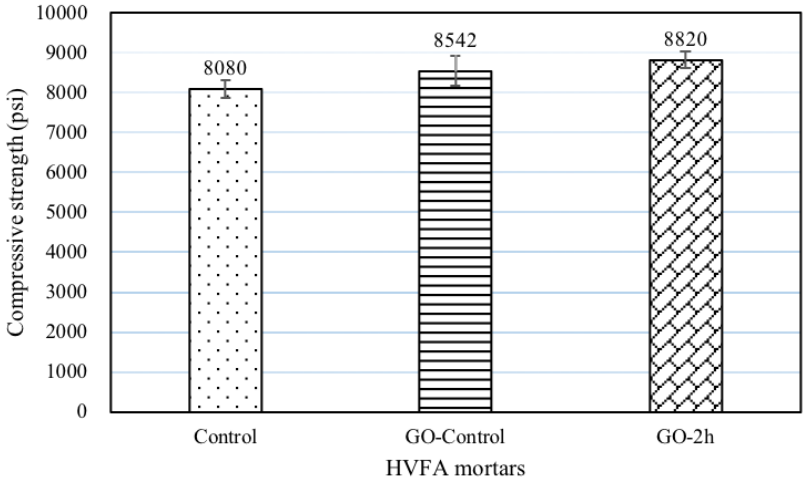


**Figure 2.11** 28-day compressive strength of HVFA mortars containing fly ash coated by GO

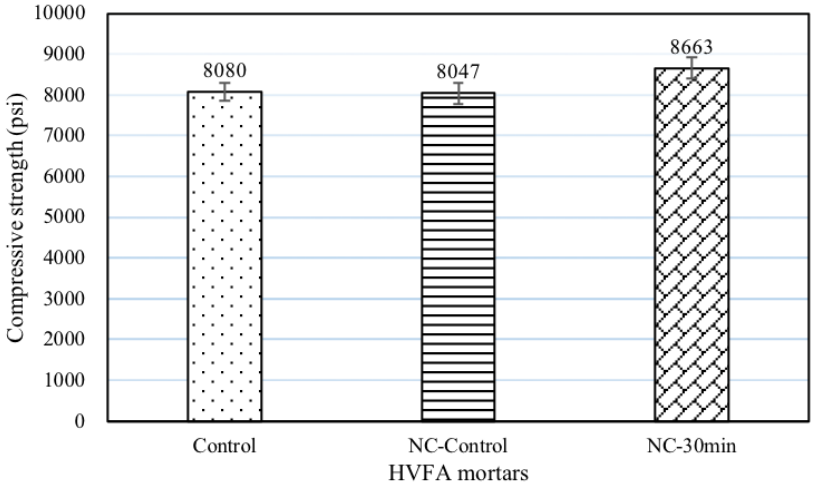


**Figure 2.12** 28-day compressive strength of HVFA mortars containing fly ash coated by NC

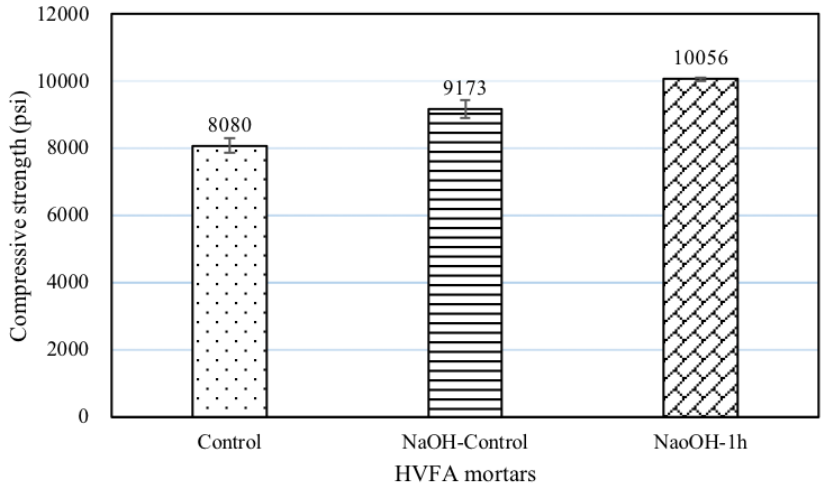


**Figure 2.13** 28-day compressive strength of HVFA mortars containing fly ash coated by NaOH

Mixtures GO-2h and NC-30min were chosen to further test their 7-day and 28-day water sorptivity and gas permeability. The results of the performance of HVFA mortars in both tests are shown in Figure 2.14 and Figure 2.15. Note that the water sorptivity coefficient examined herein is the initial rate of absorption in the first 6 hours. As expected, mixtures GO-2h and NC-30min exhibited improved transport properties, resulting from both reduced 7-day water sorptivity and gas permeability compared with mixtures GO-Control and NC-Control. However, at the curing time of 28 days, HVFA mortars showed different trends in water sorptivity and gas permeability: GO-2h and NC-30min featured decreased gas permeability but increased water sorptivity (Figure 2.15). Such different effects between the water sorptivity and gas permeability of HVFA mortars are also reported in recent research [55], which attributed the difference to the varying effects of the specific material on the reduction of capillary pore quantity and the refinement of pore structure. Some other studies [43], [50], however, reported that water absorption and gas/water permeability are related to each other. Note that both water sorptivity and gas permeability of the tested HVFA mortars decreased from 7 days to 28 days, indicating that the microstructure was denser after the initiation of pozzolanic reaction of fly ash [56].

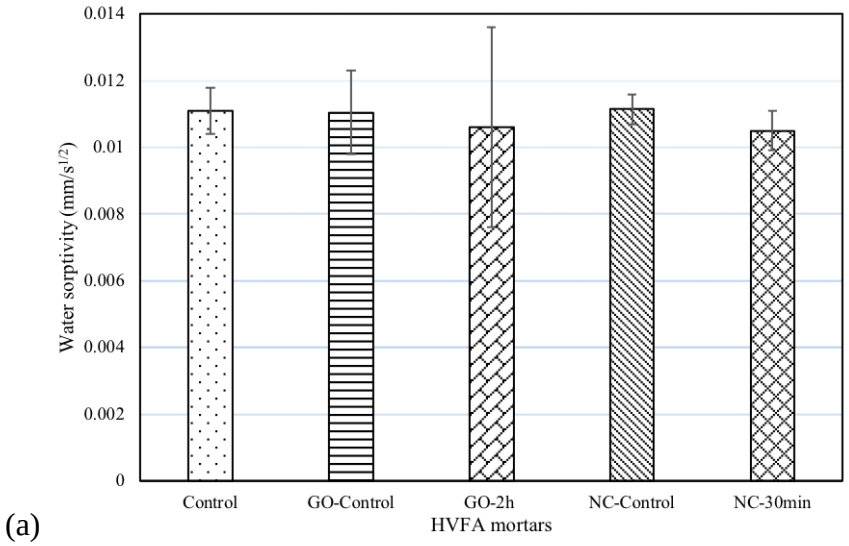


(a)

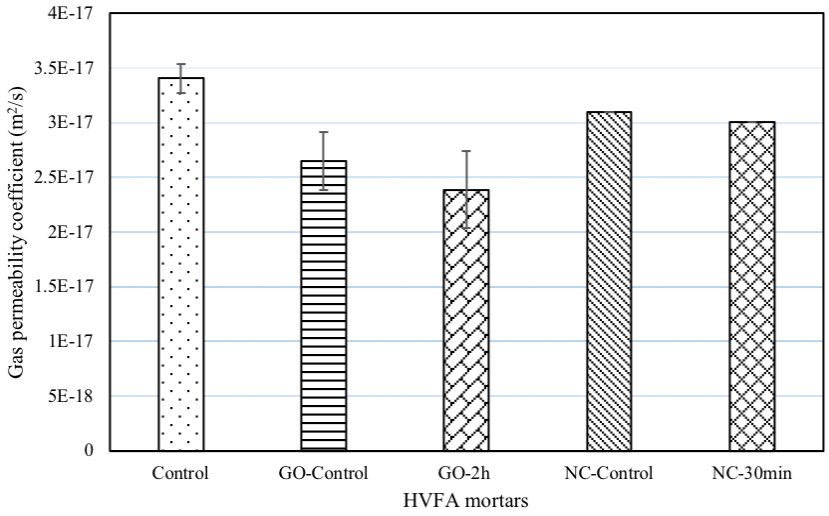


(b)

Figure 2.14 Performance of HVFA mortars at 7-day:
(a) water sorptivity and (b) gas permeability

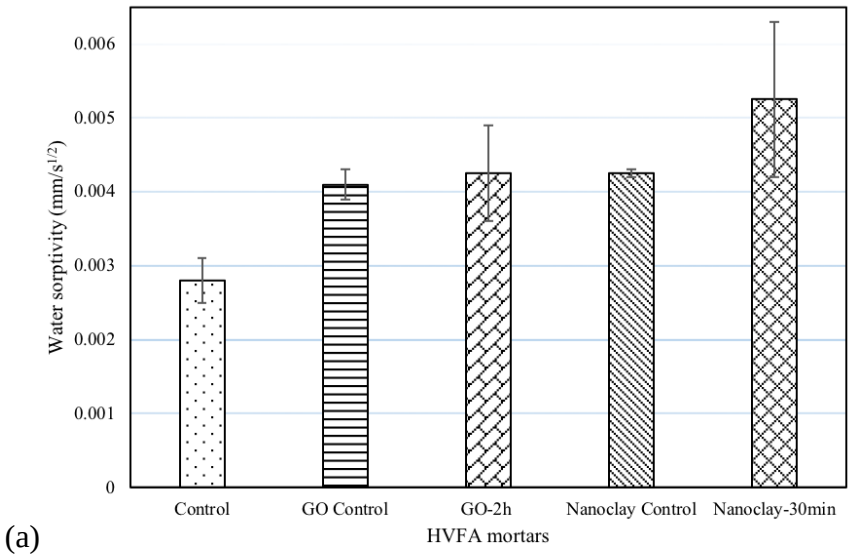


(a)

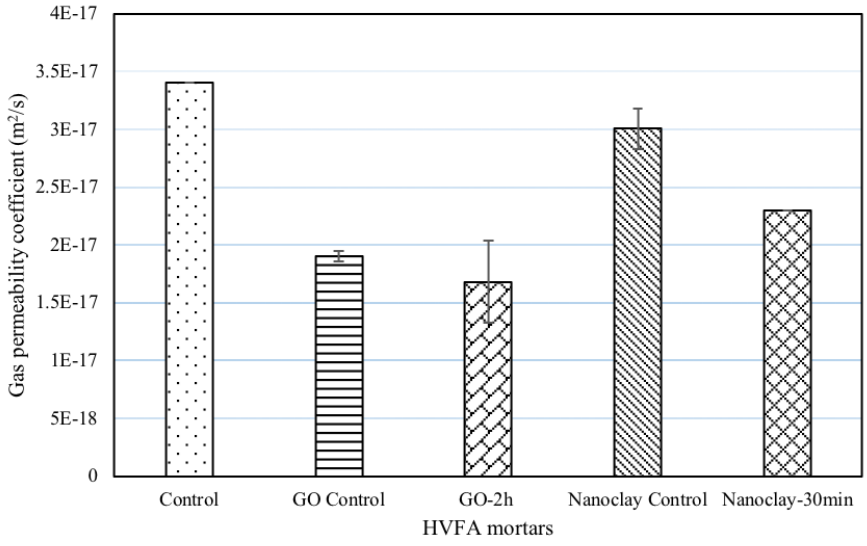


(b)

Figure 2.15 Performance of HVFA mortars at 28-day:
(a) water sorptivity and (b) gas permeability

In addition to Class F fly ash, Class C fly ash was used to investigate the effect of surface-treated fly ash on the compressive strength of HVFA mortars. In the case of Class C fly ash, which contains more CaO, the treatment time using various materials was different from that of Class F fly ash. Figure 2.16 depicts the compressive strength evolution of mixtures GO-30min, NC-30min, NaOH-1h, and their counterpart control mixtures. Similar to Class F fly ash,

the incorporation of coated Class C fly ash only improved the compressive strength of HVFA mortar at 7 days and 28 days ranging from 1.97% to 10.42%.

The results of the first trial show no significant improvement in the performance of HVFA mortars containing nanomaterial-coated fly ash particles when compared with the HVFA mortars that directly admixed nanomaterials in the mixture. In order to find the most appropriate material for coating fly ash particles, more nanomaterials in both surface treatment methods need to be explored.

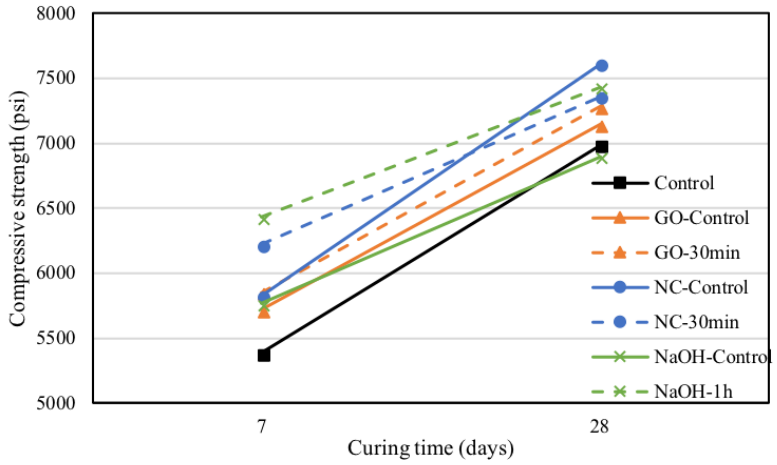


**Figure 2.16** 7-day and 28-day compressive strength of HVFA mortars containing Class C fly ash

## 2.3.2 Surface treatment of fly ash in Trial 2

In the second trial, more nanomaterials for use in the dip-coating method and more alkali solutions for use in the aqueous nanofilm growth method were employed in the selection process. Six types of new nanomaterials and two types of alkali solution were added to the HVFA mortars separately and directly at their reported optimal dosage. Both Class F and Class C fly ashes were used in HVFA mortars in the second trial. The 3-day compressive strength of HVFA mortars containing nanomaterials and alkali is illustrated in Figure 2.17. Again, a reduction in the early-age compressive strength of HVFA mortars containing Class F fly ash was

found when nanomaterials were incorporated. This finding indicates that nanomaterials mainly facilitate the activation and hydration of fly ash particles at late age. At early age, the incorporation of nanomaterials in HVFA mortars can even have an adverse effect on the compressive strength of mortar. However, for HVFA mortars containing Class C fly ash, adding the same nanomaterials increased the 3-day compressive strength of almost all mixtures. As the chemical composition and activity of fly ash varies, the effect of nanomaterials on its activation and hydration remains unknown, especially at early age, which needs more investigation.

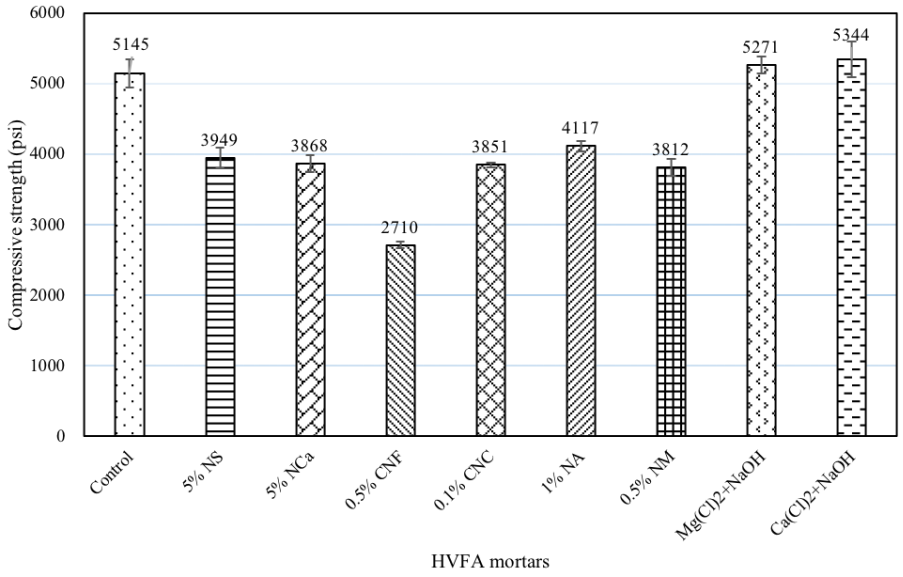


(a)

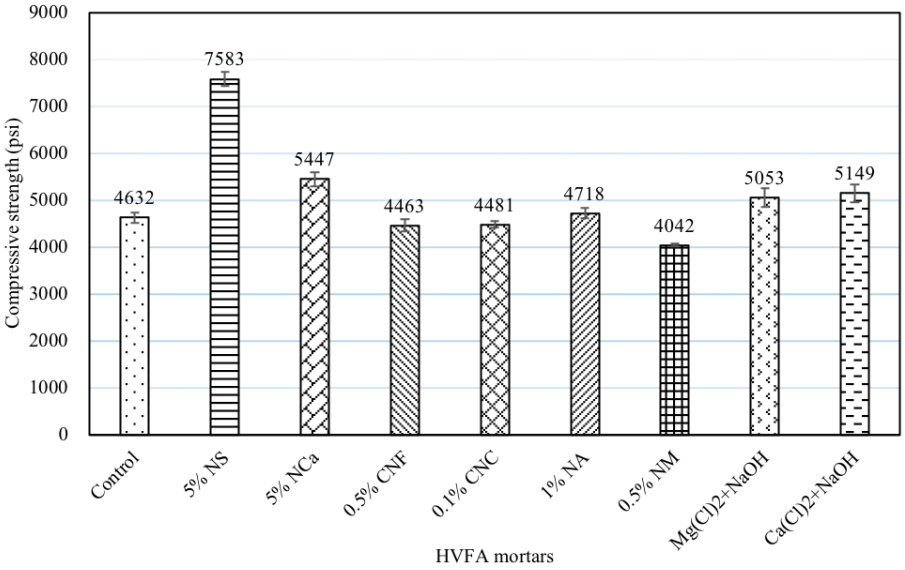


(b)

**Figure 2.17** 3-day compressive strength of HVFA mortars containing (a) Class F fly ash and (b) Class C fly ash

As it was the only nanomaterial that exhibited significant improvement in the early-age compressive strength of HVFA mortar containing Class C fly ash, nanosilica was chosen to coat fly ash particles in next step. In this study, both nanosilica powder suspension and colloid nanosilica (CNS) were explored. Colloid nanosilica is a prepared nanosilica suspension that features the benefit of avoiding agglomeration of nanomaterials [57], [58]. The fly ash particles

were treated in either type of suspension for 30 minutes, beyond which fly ash particles would agglomerate and not be suitable for the following mixing. Results of the 3-day compressive strength of HVFA mortars containing coated Class C fly ash are presented in Figure 2.18. It can be seen that no increase occurred in the compressive strength of mixtures containing fly ash particles treated by nano-$SiO_2$ or colloidal nano-$SiO_2$, compared with their control mixtures (nano-$SiO_2$ or colloidal nano-$SiO_2$ were admixed directly).

Based on the results of the first two trials, the surface treatment of fly ash particles is not an appropriate approach to improving the performance of HVFA mortars when compared with mixtures that admix treatment materials directly. The next trial, Trial 3, will focus on the surface treatment of coarse aggregate instead of fly ash particles.

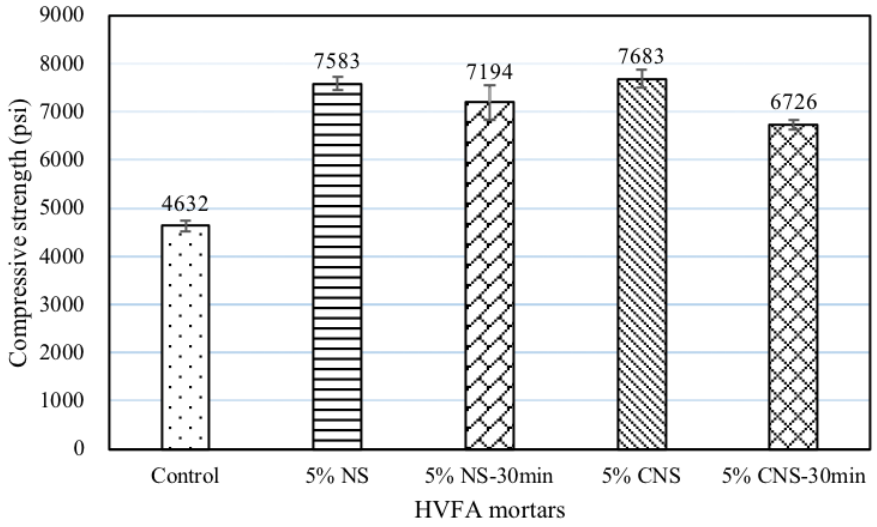


**Figure 2.18** 3-day compressive strength of HVFA mortars containing different nanosilica

2.3.3 Surface treatment of coarse aggregate in Trial 3

In the third trial, only Class C fly ash was used for casting HVFA concrete. The added nanomaterials targeted the surfaces of coarse aggregate, coating them with cement paste containing the incorporated corresponding nanomaterial. As mentioned, the Control concrete mixture was the one that coated the coarse aggregate with pure cement paste before admixing

with other components for producing HVFA concrete. Therefore, the only difference among these mixtures was the ITZ between the coarse aggregate and mortar matrix. Figure 2.19 depicts the 7-day compressive strength of four types of HVFA concrete containing various nanomaterial-coated coarse aggregate. It seems that such surface treatment produces no improvement in early-age compressive strength. Moreover, the coating of coarse aggregate by nanoclay paste imposed a negative effect on strength development, which was noticed in the first two trials also.

To better understand the effect of the improvement of ITZ on the performance of HVFA concrete, a 28-day rapid chloride migration test was conducted. The results are shown in Figure 2.20. For this test, only mixtures GO-Paste and NS-Paste were used, since they exhibited no reduced early-age compressive strength compared with the control mixture. A reduction of 8.1% and 21.5% was observed in the chloride migration coefficient for GO-Paste and NS-Paste, respectively. It is thought that there is a close relationship between the output of the rapid chloride migration test and the service life assessment of concrete structures [52], [59], especially in the environment subjected to chloride deicers. Because the coating of coarse aggregate by nanomaterial cement paste exhibited potential in extending the service life of HVFA concrete pavement in de-icing salt environments, this approach was selected for further investigation (details found in Chapter 3).

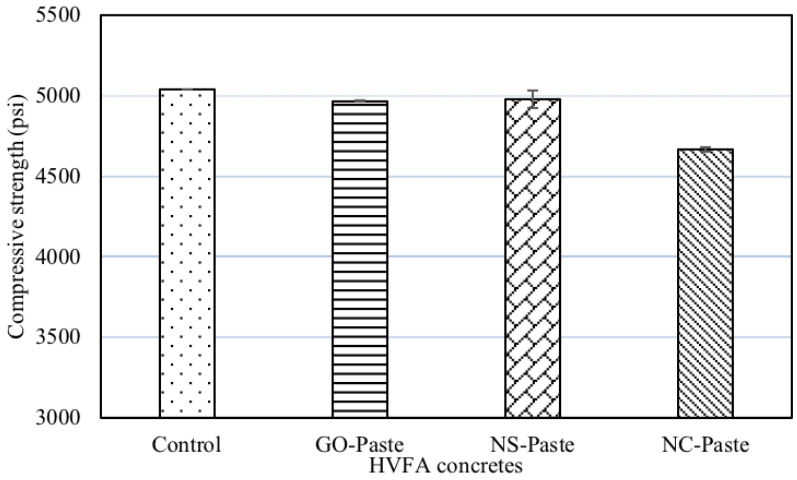


**Figure 2.19** 7-day compressive strength of HVFA concretes

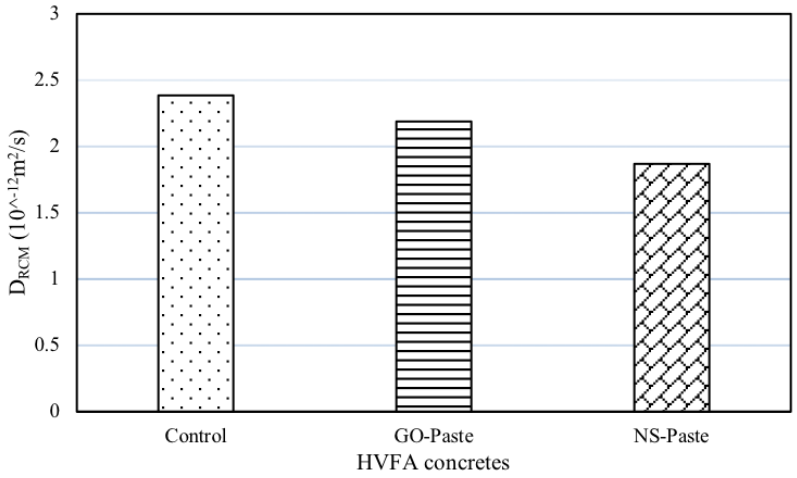


**Figure 2.20** 28-day chloride migration coefficient of HVFA concretes

## 2.4 Summary and Conclusions

This chapter explored three surface treatments, using dip-coating or aqueous nanofilm growth: the first two trials for fly ash particles and the third trial for coarse aggregate. Both Class F fly ash and Class C fly ash were treated with various nanomaterials in the fly ash treatment process, while coarse aggregate with a maximum size of 3/4 inch was coated in the third trial by cement paste that featured a lower water/cement ratio and contained nanomaterials at their optimum dosages.

In the first trial, an increase, but not a significant one, was observed in the 7-day compressive strength of HVFA mortars containing treated Class F fly ash particles when compared with mixtures that directly admixed nanomaterials (12.6%, 18.1%, and –4.2% for GO-2h vs. GO-Control, NC-30min vs. NC-Control, and NaOH-1h vs. NaOH-Control, respectively). However, for 28-day compressive strength, the NaOH-1h mixture showed the greatest improvement (9.6%) of the three mixtures. In addition to investigating compressive strength, 7- and 28-day water sorptivity and gas permeability of the mixtures were investigated. Unfortunately, no significant improvement was observed in such properties of HVFA mortars. Similar results were obtained for HVFA mortars containing Class C fly ash; that is, no significant improvement was observed in compressive strength.

In addition to graphene oxide, nanoclay, and NaOH, eight other nanomaterials (nano-$SiO_2$, nano-$CaCO_3$, cellulose nanofiber, cellulose nanocrystal, nano-$Al_2O_3$, nanomontmorillonoid, $Mg(Cl)_2$+NaOH, and $Ca(Cl)_2$+NaOH) were admixed directly into HVFA mortar containing both Class F and Class C fly ash particles without any treatment in the second trial. Only 5% nano-$SiO_2$ showed a significant increase (63.7%) in the 3-day compressive strength of Class C HVFA mortar. However, no increase was observed in the compressive strength of mixtures containing fly ash particles treated by nano-$SiO_2$ or colloidal nano-$SiO_2$ compared with their control mixtures (with nano-$SiO_2$ or colloidal nano-$SiO_2$ admixed directly).

Although no improvement was observed in the early-age compressive strength of the HVFA concrete made with coarse aggregate that was coated by nanomaterial-added cement paste, the chloride migration coefficient of such concrete was reduced compared with concrete produced with coarse aggregate coated by pure cement paste. The reduced chloride migration

coefficient was related to the longer service life of HVFA concrete, especially in environments where concrete is subjected to de-icing salts.

The surface treatment of coarse aggregate was chosen as the best appropriate method for improving the performance of HVFA concrete. Chapter 3 details the effect of this surface treatment method on the mechanical properties, transport properties, and freezing/thawing resistance of HVFA concrete.

# CHAPTER 3 HVFA CONCRETE CONTAINING COATED COARSE AGGREGATE

## 3.1 Introduction

It is well recognized that the interfacial transition zone (ITZ)—the area between aggregate and cement paste—is one of the most vulnerable areas of concrete [60]. Under compression loading, concrete exhibits quasi-ductile behavior due to the presence of the ITZ (Figure 3.1). Multiple micro-cracks occur in the ITZ when loading occurs beyond the bearing capacity of concrete [61], which confirms the ITZ as the weak link in concrete. In fact, the microstructure, chemistry, and porosity of this interface influence the bond between aggregates and paste and, therefore, affect the performance of concrete under certain conditions. The traditional strategy for improving the ITZ has been the addition of pozzolanic materials [60] and nanomaterials [62]. However, when added, these materials end up in the bulk of the cement paste matrix. An investigation into a method that targets additives to the ITZ or the surface of aggregates is needed.

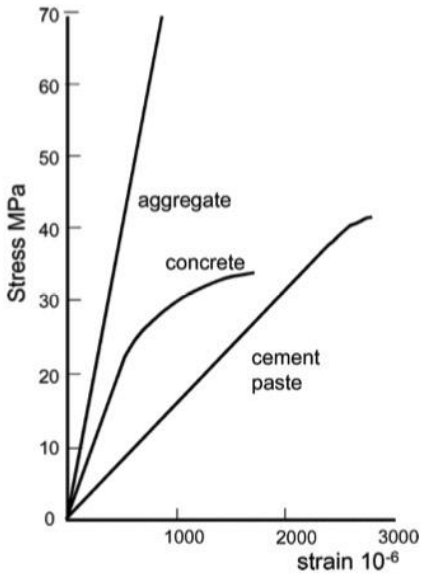


**Figure 3.1** Comparative stress strain curves for aggregate, paste, and concrete [61]

Aiming at improving the ITZ of concrete or mortar by using a small dosage of additives, many researchers have focused on dip-coating the sand by nanomaterial sol [60] or soaking the recycled aggregate in nanomaterial slurry and cement slurry [63], [64]. These surface treatments can significantly improve the quality of corresponding mortar or concrete with the help of proper mixing approaches. The new ITZ between the coated aggregate and paste can also be enhanced by such treatments. This chapter reports on the investigation into the effect of the surface treatment method (see Chapter 2) selected for testing the mechanical properties, transport properties, and freezing/thawing resistance of HVFA concrete. The microstructure and chemistry of the ITZ in untreated and treated concrete samples were also investigated, using SEM/EDS techniques.

## 3.2 Experimental Program

### 3.2.1 Materials

The same cement, sand, and coarse aggregate detailed in Chapter 2 were used in this section of the study. Because Class C fly ash exhibited more pozzolanic reaction potential, it was the only supplementary cementitious material (SCM) used in mixing of HVFA concrete.

### 3.2.2 Surface treatment on coarse aggregate

The surface treatment method tested in Trial 3 (see Chapter 2) that improved the chloride migration resistance of HVFA concrete was used. Three types of slurries containing different nanomaterials were prepared. The first slurry, labeled Control, only contained cement and water. Graphene oxide (GO) and nanosilica (NS) were added to the other two cement slurries at dosages of 0.1% and 1%, respectively, at the weight of cement. These two slurries were labeled GO slurry and NS slurry. The proportions of the components contained in the three types of slurries are provided Table 3.1.

**Table 3.1** Proportions of the three slurries prepared

| Paste slurry | Cement ($kg/m^3$) | Water ($kg/m^3$) | W/C | GO ($kg/m^3$) | NS ($kg/m^3$) | Superplasticizer ($mL/m^3$) |
|---|---|---|---|---|---|---|
| Control | 500 | 125 | 0.25 | 0 | 0 | 6000 |
| GO slurry | 500 | 125 | 0.25 | 0.5 | 0 | 10000 |
| NS slurry | 500 | 125 | 0.25 | 0 | 5 | 10000 |

Surface treatment of coarse aggregate was achieved by pouring the corresponding slurries on the aggregate. First, the nanomaterials were dispersed in water. Afterward, three types of cement slurry with good dispersion were prepared by mixing the cement with water or nanomaterial suspensions for 2 minutes. Then the obtained slurry was poured on the surface of untreated coarse aggregate, and the aggregate was coated by spreading it out. The final step of the process was to dry the coarse aggregate at room temperature for about 4 hours. The untreated

and treated coarse aggregate are shown in Figure 3.2, from left to right. Figure 3.2 demonstrates that, after treatment, a coating formed on the surface of the coarse aggregate.

**Figure 3.2** Coarse aggregate before and after (left to right) surface treatment using cement slurry

### 3.2.3 Mixing proportions

By using the four groups of coarse aggregate (untreated, treated by cement, GO, and NS slurries), a total of five groups of concrete mixtures were produced, including one ordinary Portland cement (OPC) concrete and four HVFA concrete mixtures. Mixing proportions of the five concrete groups are illustrated in Table 3.2. A series of 101.6 mm (diameter) × 203.2 mm (height) cylinders were prepared for each group. Prism samples with size of 76 × 102 × 406 mm (3 × 4 × 16 in.) were also cast for the freezing and thawing (F-T) test. After casting, all samples were covered with plastic membrane and left at room temperature for 24 hours. Then the concrete samples were demolded and cured in a wet chamber (temperature: 22 ± 2°C, relative humidity: 98%) for a specific number of days before further testing.

**Table 3.2** Mixture proportions of the five concrete groups

| Concrete Mixes | Cement | Class C Fly Ash | Water | W/B | Fine Aggregate | Coated Coarse Aggregate | Superplasticizer ($mL/m^3$) |
|---|---|---|---|---|---|---|---|
| OPC-Control | 500 | 0 | 200 | 0.4 | 750 | 750 | 625 |
| HVFA-Control | 200 | 300 | 150 | 0.3 | 750 | 750 | 1750 |
| HVFA-Coat-Control | 200 | 300 | 150 | 0.3 | 750 | 750 | 2000 |
| HVFA-GO-Coat | 200 | 300 | 150 | 0.3 | 750 | 750 | 2250 |
| HVFA-NS-Coat | 200 | 300 | 150 | 0.3 | 750 | 750 | 2250 |

### 3.2.4 Test methods

Compressive strength and splitting strength were tested by curing for 3, 7, 14, and 28 days using a SATEC compression test machine, following ASTM C109 and C1006. Both strengths provide a macroscopic indication of cementing ability of HVFA binder and the effect of surface treatment of coarse aggregate on mechanical properties of HVFA concrete.

The water sorptivity test was conducted at 28 days, using the same procedure detailed in Chapter 2; the specimens used were 50 mm thick slices cut from the middle part of each cylinder concrete sample.

The chloride migration coefficient obtained from the RCM test was employed to characterize the 28-day transport property of the HVFA concrete related to chloride migration. The procedure described in Chapter 2 was used here as well.

Prism samples were cured in the wet chamber for 14 days before performing the F-T test, following the ASTM C666 standard. One day prior to the test, samples were soaked in water for 24 hours to test their initial fundamental transverse frequencies and masses. Afterward, samples were subjected to F-T cycles at the beginning of the thawing phase of the cycles. The temperature range of every F-T cycle was measured using a thermocouple embedded in the

concrete samples (Figure 3.3). The thermocouples were embedded in the center part of the sample, where the temperature measured was more accurate for samples in the F-T chamber. The F-T rate of the sample was also recorded by the thermocouple. In Figure 3.4, it can be seen that the temperature range of each F-T cycle was between -22°C and 9°C. The rate of the temperature change was 7.6°C/h at the freezing phase and 25.8°C/h at the thawing phase, respectively. A F-T cycle took about 5 hours and 10 minutes, resulting in about 4.6 cycles per day. After every 29 cycles (1 week), samples in thawing condition were removed from the chamber and tested for fundamental transverse frequency and mass. Then the samples were returned to positions according to the predetermined rotation scheme that would ensure that each sample was subjected to conditions in all parts of the freezing chamber. The relative dynamic modulus of elasticity of the samples can be calculated using the following equation, according to ASTM C666:

$$P_c = (n_1^2/n^2) \times 100 \quad (3)$$

where $P_c$ is the relative dynamic modulus of elasticity after $c$ cycles of F-T (%), $n$ is the initial fundamental transverse frequency, and $n_1$ is the fundamental transverse frequency after $c$ cycles of F-T.

**Figure 3.3** Thermocouples embedded concrete samples in the F-T chamber

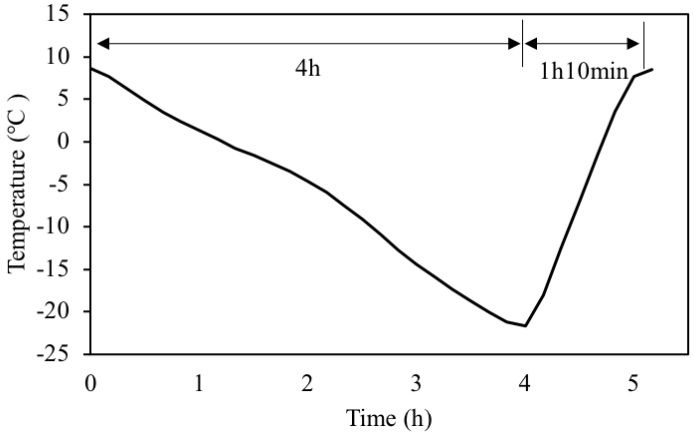


**Figure 3.4** Temperature profiles for F-T test

To examine the microstructure of concrete samples at the curing time of 28 days, a JEOL JXA-8500F electron microprobe was employed. Each specimen examined was a slice about 1 cm × 1 cm in size, cut from the middle part of the cylinder concrete. After having been cut, the specimen was dried, impregnated with low-viscosity epoxy resin, and successively polished with oil-based diamond powder. Then the sections were coated with carbon, before being subjected to the field emission electron probe microanalyzer. This machine was coupled with an energy

spectrum transmitter, which enables energy dispersive X-ray spectroscopy (EDS). Specifically, a microanalytical unit allowed the detection of small variations in trace element content, using a scan time of 60 seconds per sampling area at the accelerating voltage of 20 kV.

## 3.3 Results and Discussion

### 3.3.1 Compressive strength and splitting tensile strength

Test results of compressive strength and splitting tensile strength for all five groups of concrete are shown in Table 3.3 and

Table **3.4**, as well as in Figure 3.5 and Figure 3.6. As seen in Table 3.3 and Figure 3.5, the concrete samples containing nanomaterial-coated coarse aggregate show almost the same compressive strength as the concrete samples containing coarse aggregate that is coated with pure cement paste or even uncoated coarse aggregate at the curing age of 3 days to 28 days. This finding was expected, as this surface treatment approach exhibited no improvement in 7-day compressive strength in the third trial (see Chapter 2). Other studies, [60], [64], [65], however, indicate that a small dose of surface treatment materials significantly improved the mechanical properties of corresponding concrete or mortar. This result needs further investigation on the ITZ of the obtained concretes. When compared with OPC concrete, all HVFA concretes exhibited comparable or even higher compressive strength tested at various curing ages. Although the compressive strength development at early age was slower than OPC concrete, HVFA concretes featured rapid strength evolution at later age (from 14 days to 28 days), which was found in other research as well [66], [67].

From the results of the splitting tensile strength tests (

Table **3.4** and Figure 3.6), one can see that only mixtures HVFA-GO-Coat and HVFA-NS-Coat had strength comparable to OPC concrete;  other HVFA mixtures showed lower

strength, especially at the curing time of 28 days. This result may be attributed to the improvement in the ITZ of concrete containing coated coarse aggregate, which increased the bond between aggregate and paste and thus the resistance to splitting under loading.

**Table 3.3** Compressive strength of concrete in the testing groups (psi)

| Concrete Mixes | 3 Days | 7 Days | 14 Days | 28 Days |
|---|---|---|---|---|
| OPC-Control | 3956.8 | 4962.1 | 5926.6 | 6255.1 |
| HVFA-Control | 4274.0 | 4919.6 | 5193.0 | 6170.1 |
| HVFA-Coat-Control | 4348.2 | 4909.0 | 5510.6 | 6276.8 |
| HVFA-GO-Coat | 4113.5 | 4817.0 | 5294.1 | 5999.9 |
| HVFA-NS-Coat | 4168.7 | 5012.5 | 5550.8 | 6295.5 |

**Table 3.4** Splitting tensile strength of concrete in the testing groups (psi)

| Concrete Mixes | 3 Days | 7 Days | 14 Days | 28 Days |
|---|---|---|---|---|
| OPC-Control | 350.9 | 380.0 | 456.4 | 563.5 |
| HVFA-Control | 388.9 | 404.7 | 494.0 | 500.3 |
| HVFA-Coat-Control | 416.6 | 435.5 | 449.1 | 457.7 |
| HVFA-GO-Coat | 373.3 | 483.5 | 490.5 | 567.9 |
| HVFA-NS-Coat | 415.8 | 415.0 | 479.5 | 548.6 |

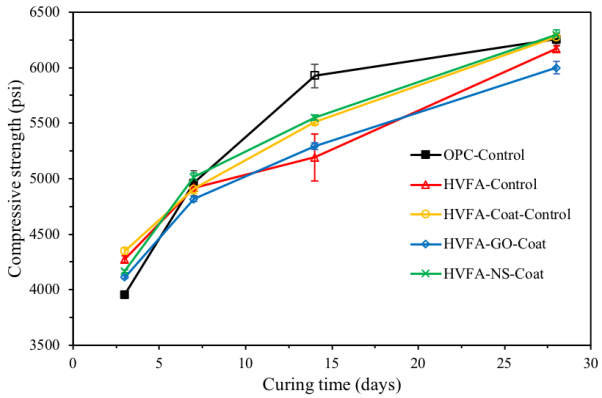


**Figure 3.5** Compressive strength (from 3 days to 28 days) of concrete in five groups

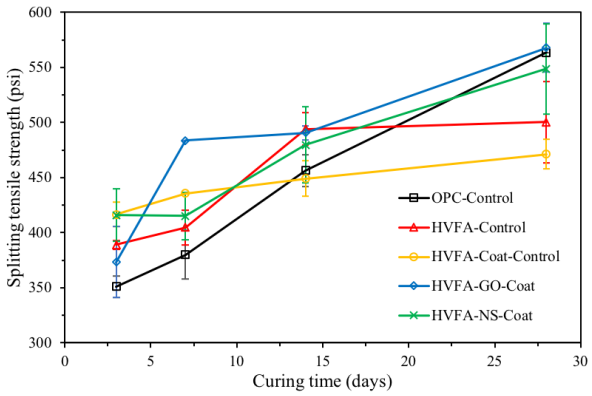


**Figure 3.6** Splitting tensile strength (from 3 days to 28 days) of concrete in five groups

### 3.3.2 Water sorptivity

Water sorptivity is defined by the rate of water absorption due to capillary action [49]. Water absorption over time for the five concrete mixtures is depicted in Figure 3.7, which suggests that the water absorption of the concrete increased sharply in the first 6 hours and then, after the first day, water absorption became increasingly stable. When HVFA was incorporated in the concrete, the mixtures showed much less water absorption, which was consistent with the findings of other research [68], [69]. In general, the use of fly ash in concrete can result in pore refinement, and thus reduced permeability of concrete [70].

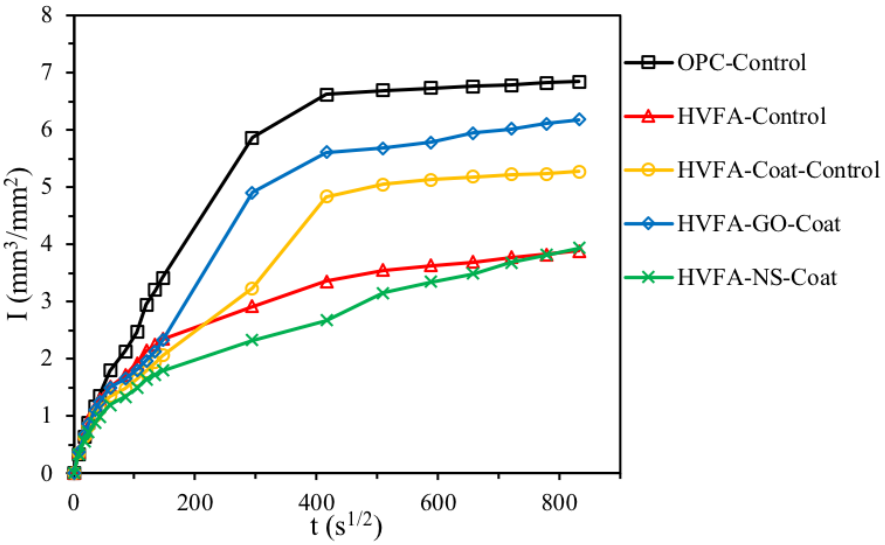


**Figure 3.7** The overall relationship between water absorption amount and time of concretes

Figure 3.8 focuses on the initial absorption period. The water sorptivity coefficient $k_s$ of different mixtures was calculated as the slope of the linear fit, as shown in Figure 3.8 and Table 3.5. Note that the sorptivity coefficient of the HVFA concrete mixtures was significantly smaller than that of OPC concrete. The $k_s$ obtained from the HVFA concrete was only 49%~64% of the counterpart calculated from OPC concrete. This likely resulted from the denser microstructure and refined pore structure of HVFA concrete compared with OPC concrete at the same strength [10]. Among the HVFA concrete mixtures, HVFA-NS-Coat exhibited the best performance in water sorptivity, as it featured the lowest sorptivity coefficient. This result confirmed that the surface treatment of coarse aggregate by using nanomaterial-incorporated cement paste is an effective approach in improving the transport property of HVFA concretes.

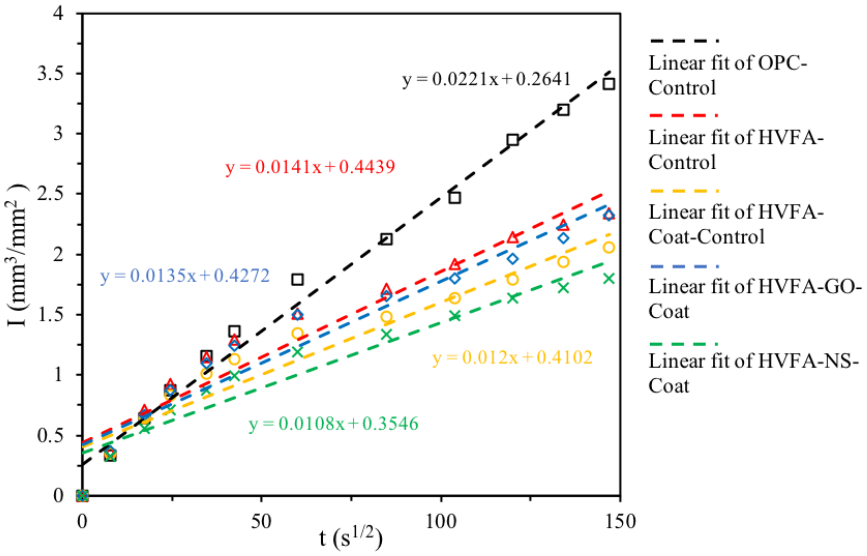


**Figure 3.8** The linear range relation between water absorption amount and time of concretes

**Table 3.5** Water sorptivity coefficient of different concretes

| Mixtures | OPC-Control | HVFA-Control | HVFA-Coat-Control | HVFA-GO-Coat | HVFA-NS-Coat |
|---|---|---|---|---|---|
| $k_s$ (mm/s$^{1/2}$) | 0.0221 | 0.0141 | 0.012 | 0.0135 | 0.0108 |

### 3.3.3 Rapid chloride migration

A non-steady-state testing regime could lead to rapid determination of chloride migration in treated and untreated concretes [71]. The Nord Test Standard 492 utilizes NaCl and NaOH solutions in combination with an applied voltage to electrochemically introduce chlorides to a concrete specimen. After the treatment period (usually 24 hours), the specimen is split and silver nitrate solution is used to precipitate chlorides, resulting in a measurable "reaction front" (Figure 3.9).

**Figure 3.9** Precipitated chlorides after treatment with silver nitrate (arrow indicates precipitated chlorides reaction front)

Table 3.6 presents the depth of chloride penetration and the corresponding chloride migration coefficient $D_{RCM}$ of the tested concrete samples. It is known that applied voltage has an influence on the value of chloride migration coefficient determined by the RCM test [52]. Note that the applied voltage was related to the initial current passed through the concrete samples, which was adjusted by the voltage to lie in a normal range. The results shown in Table 3.6 indicate that HVFA concretes exhibited significantly reduced chloride migration coefficient

compared with OPC concrete. The reduced chloride penetration of HVFA concrete was also found in many other studies [7], [69], [72]. The incorporation of fly ash at high volume in concrete can facilitate the formation of denser microstructure in concrete [73], or allow the concrete higher chloride binding capacity due to the alumina in fly ash [74], both of which increase resistance to chloride penetration. By employing surface-treated coarse aggregate, the resistance of HVFA concrete to chloride diffusion was improved. Such results are closely related to the enhancement of the ITZ in concrete, which helps reduce the penetration paths of chloride [64]. The modification effects of the nanosilica-containing cement paste on the concrete's resistance to chloride diffusion were better than the modification effects of graphene oxide-containing cement paste. Mixture HVFA-NS-Coat had a 35.8% decrease in penetration compared with control mixture HVFA-Control. This decrease is significant, since the mix design includes only a very small amount of $SiO_2$ nanoparticles. Although ITZ pore connectivity is not the only cause of chloride diffusion [75], the nanosilica-containing cement paste was either creating barriers in the ITZ or chemically blocking the diffusion of chloride ion through the matrix.

**Table 3.6** Results of RCM testing of different concretes

| Sample | Depth of Chloride Penetration (mm) | Applied Voltage (V) | $D_{RCM}$ ($10^{\wedge -12}$) |
|---|---|---|---|
| OPC-Control | 13.9 | 10 | 18.35 |
| HVFA-Control | 6.4 | 25 | 3.10 |
| HVFA-Coat-Control | 4.7 | 25 | 2.18 |
| HVFA-GO-Coat | 4.9 | 25 | 2.24 |
| HVFA-NS-Coat | 5.7 | 35 | 1.99 |

### 3.3.4 Freezing-thawing cycles

As is well known, HVFA concrete usually performs poorly in freezing and thawing (F-T) tests and salt scaling tests [76], [77]. One possible reason is the loss of air-entraining agent to the free carbon in fly ash [78]. Generally, the extent of surface scaling is greatly affected by the intrinsic transport properties of concrete [79]. In order to investigate the effect of surface treatment on coarse aggregate on the resistance of HVFA concrete to F-T cycles, mixtures that were not air-entrained were investigated.

Figure 3.10 illustrates that the weight change of the concrete mixtures during the F-T test, in which the number of F-T cycles that each mixture exposed was up to the specific value when its dynamic elastic modulus reached 60% of the initial value. In the first 58 F-T cycles, almost all the mixtures exhibited a weight gain. This is mainly attributed to the water absorption in the thawing condition [78]. Since the HVFA concrete samples were subjected to the F-T cycles at the curing age of 14 days, the moisture uptake may occur in concrete for the pozzolanic reaction of fly ash particles. After 348 F-T cycles, when the relative dynamic elastic moduli of mixtures HVFA-GO-Coat and HVFA-NS-Coat reached the value below 60% of their initial moduli, respectively, the record of the weight loss of the HVFA concrete mixtures was stopped. A weight loss of 9.5% was observed for the mixture HVFA-GO-Coat, while only 6.8% loss in weight was measured in the mixture HVFA-NS-Coat. Surface coating on coarse aggregate by nanosilica-containing cement paste significantly extended the service life of HVFA concrete in the cold climate, at a cost of not losing a significant amount of substance in the surface.

The degradation of dynamic elastic modulus of concrete subjected to F-T cycles is shown in Figure 3.11. With an increasing number of F-T cycles, the dynamic elastic moduli of all mixtures decreased. Compared with OPC concrete, all the HVFA concrete mixtures exhibited

slower reduction speed in the dynamic elastic moduli, which translated to a better F-T resistance. This result is consistent with many other researches and can be explained by the improved transport and permeability properties of HVFA concretes. Moreover, the surface treatment on coarse aggregate enabled HVFA concretes a further improved resistance in F-T test, especially for HVFA concretes containing NICP-CCA. About 210 cycles and 330 cycles were observed for mixtures HVFA-Coat-Control and HVFA-NS-Coat, respectively, when their relative dynamic elastic moduli reached 60%. This result demonstrates the benefits of the surface treatment on coarse aggregate by nanosilica-containing cement paste on the F-T resistance of HVFA concrete.

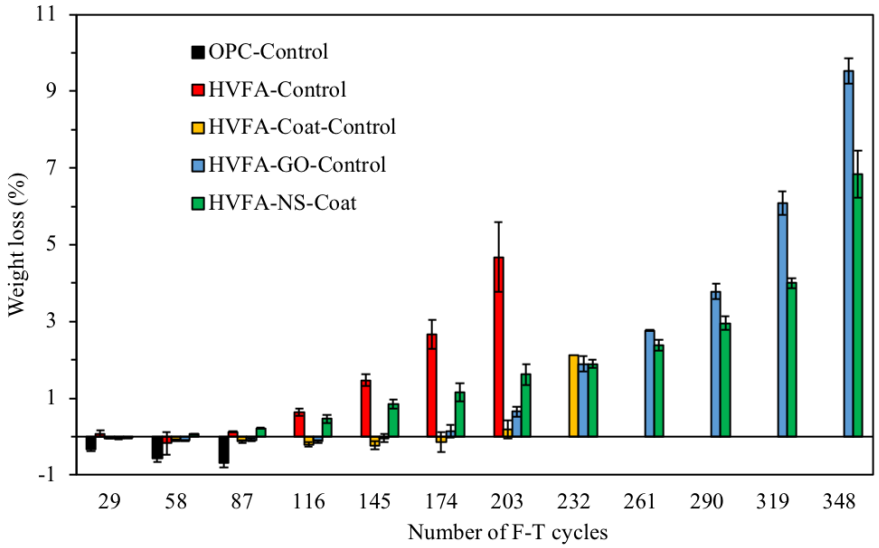


**Figure 3.10** Weight loss of concretes subjected to different F-T cycles

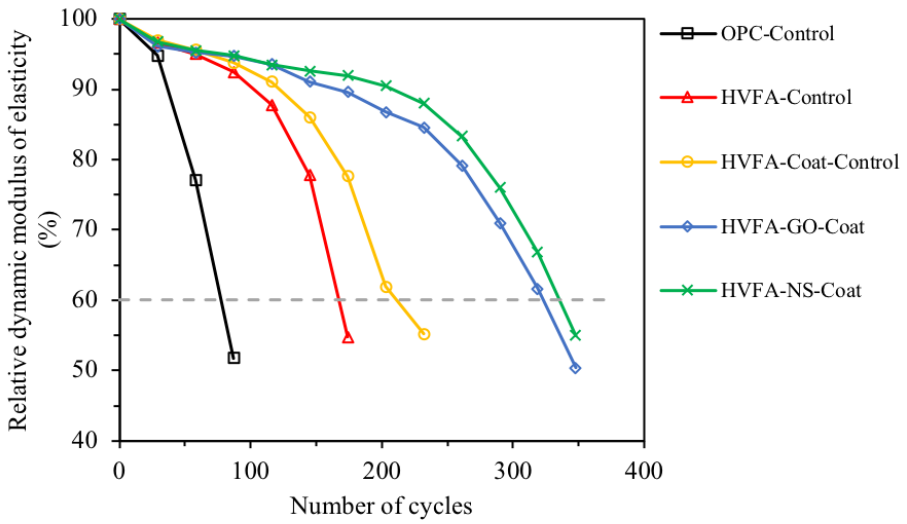


**Figure 3.11** Relative dynamic elastic modulus of concrete subjected to different F-T cycles

### 3.3.5 Microstructure investigation

Generally, nanoparticles added when mixing concrete affect only the microstructure of the paste matrix, without making any significant improvement in the ITZ of the concrete. The addition of nanoparticles as thin film on the aggregate surface before concrete is manufactured is considered an effective approach to improving the ITZ and thereby the performance of concrete [65]. For coating coarse aggregate by nanosilica-containing cement paste in HVFA concrete, the ITZ was improved by reducing the porosity in the ITZ, as clearly presented in Figure 3.12. Compared with mixtures HVFA-Control and HVFA-Coat-Control, mixture HVFA-NS-Coat featured much denser ITZ between the coarse aggregate and the paste matrix. Typically, the ITZ locates in the area within 50 μm from the interface [61]. Half of the spots in Figure 3.12 were chosen for EDS analysis.

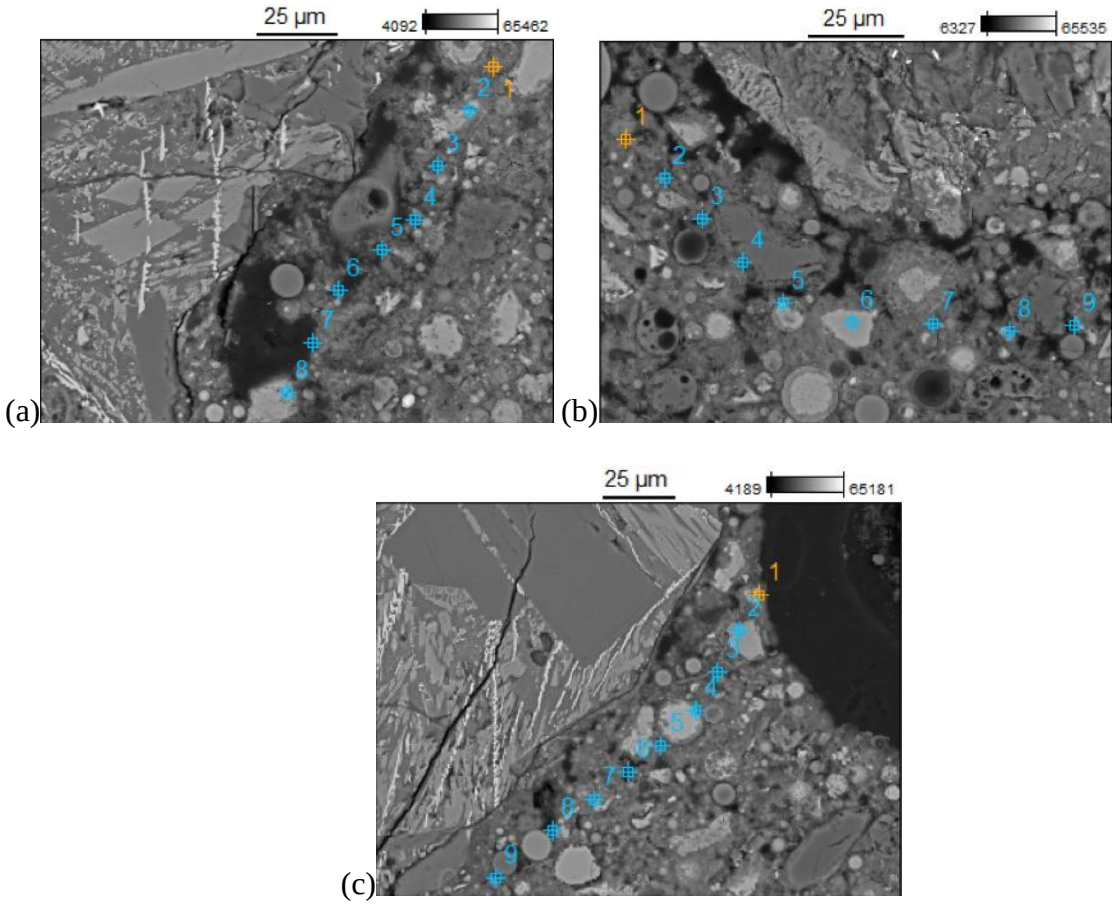


**Figure 3.12** SEM images of ITZs for (a) HVFA-Control, (b) HVFA-Coat-Control, and (c) HVFA-NS-Coat

Besides the spots shown in Figure 3.12, another two areas in the ITZ and three areas in the paste in each mixture were randomly selected for the element composition distribution analysis. Spots numbered in the selected area were set as 8 or 9, each of them uniformly distributed in the interest area. The content of four primary chemical elements, Al, Si, S, and Ca, were obtained from the EDS data; they are illustrated as box plots in Figure 3.13, Figure 3.14, and Figure 3.15. As seen in these figures, mixture HVFA-NS-Coat featured higher Ca and lower Al contents in the ITZ than mixtures HVFA-Control and HVFA-Coat-Control, suggesting that the hydration products in the ITZ were altered by the surface treatment. In all HVFA concrete, there were similar levels of Si and S content shown in the ITZ or paste area.

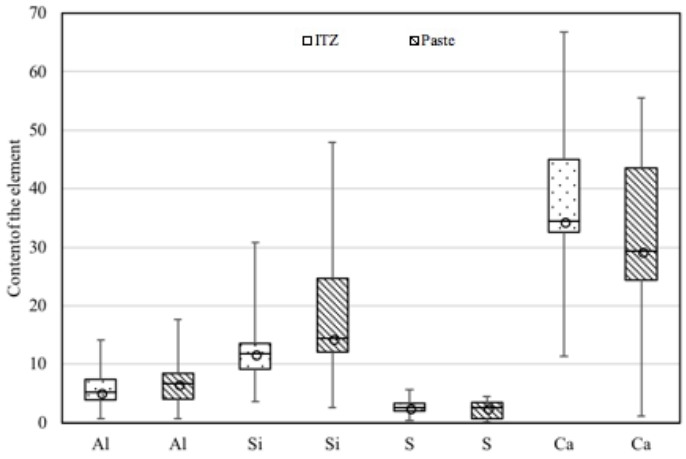


**Figure 3.13** Box plot of the key element contents in the ITZ and paste of mixture HVFA-Control

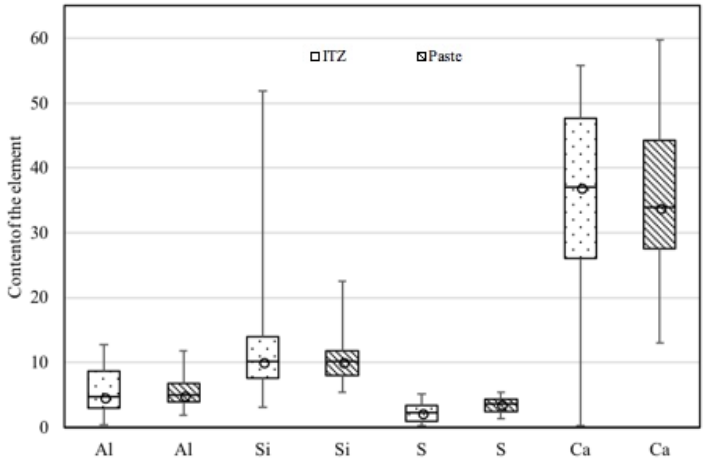


**Figure 3.14** Box plot of the key element contents in the ITZ and paste of mixture HVFA-Coat-Control

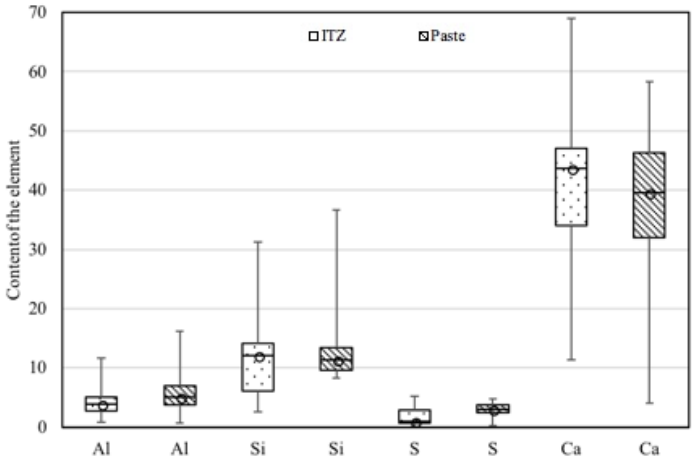


**Figure 3.15** Box plot of the key element contents in the ITZ

and paste of mixture HVFA-NS-Coat

Mole ratios of the aforementioned primary elements were generated by processing the EDS data from each element content. Figure 3.16, Figure 3.17, and Figure 3.18 present the box plots of Ca/Si, Ca/(Si+Al), Al/Si, and S/Si mole ratios in the ITZ and paste area in three HVFA mixtures. Compared with mixtures HVFA-Control and HVFA-NS-Coat, which featured Ca/Si ratio in the ITZ mostly in the range of from 1.9 to 3.0 and from 2.7 to 3.7, and with the median value of 2.4 and 3.0, respectively, mixture HVFA-NS-Coat exhibited a lower ratio of from 2.1 to 2.9 and median value of 2.3. It is known that $Ca(OH)_2$ generally has a Ca/Si mole ratio greater than 2 [80]. Therefore, the treatment of the surface of coarse aggregate by using nanosilica-containing cement paste reduced the content of $Ca(OH)_2$, which was consumed by the pozzolanic reaction. This result is confirmed by the improved ITZ and dense microstructure observed in the SEM images. It is noteworthy that the Al/Si ratio in the ITZ of mixture HVFA-NS-Coat was much lower than that in the other two mixtures, suggesting the generation of calcium-alumina-silicate-hydrate (C-A-S-H) in the ITZ of the treated concrete. The more hydration products present in the ITZ, the denser the microstructure of ITZ becomes and, therefore, the better the performance of the concrete.

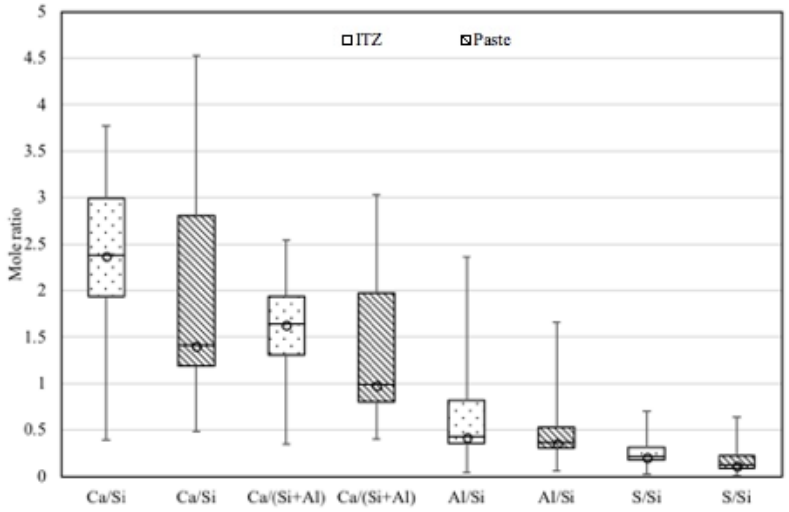


**Figure 3.16** Box plot of Ca/Si, Ca/(Si+Al), Al/Si, and S/Si mole ratio in the ITZ and paste of mixture HVFA-Control

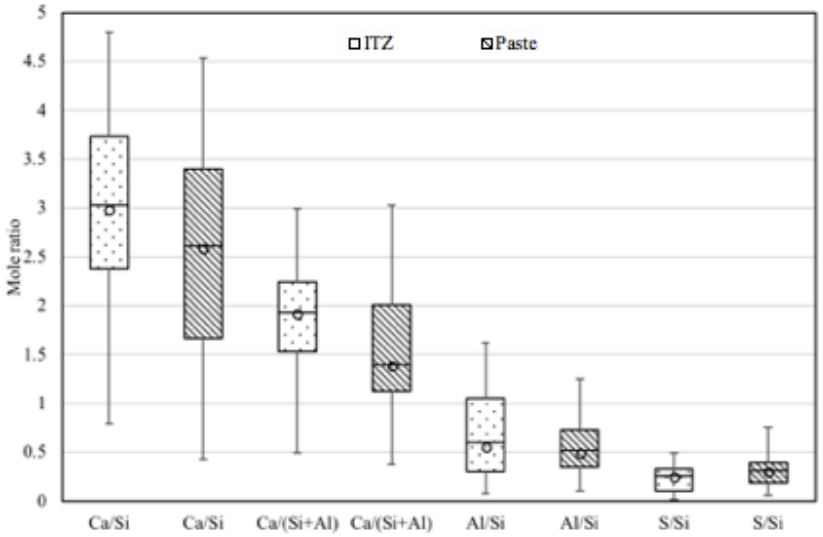


**Figure 3.17** Box plot of Ca/Si, Ca/(Si+Al), Al/Si, and S/Si mole ratio in the ITZ and paste of mixture HVFA-Coat-Control

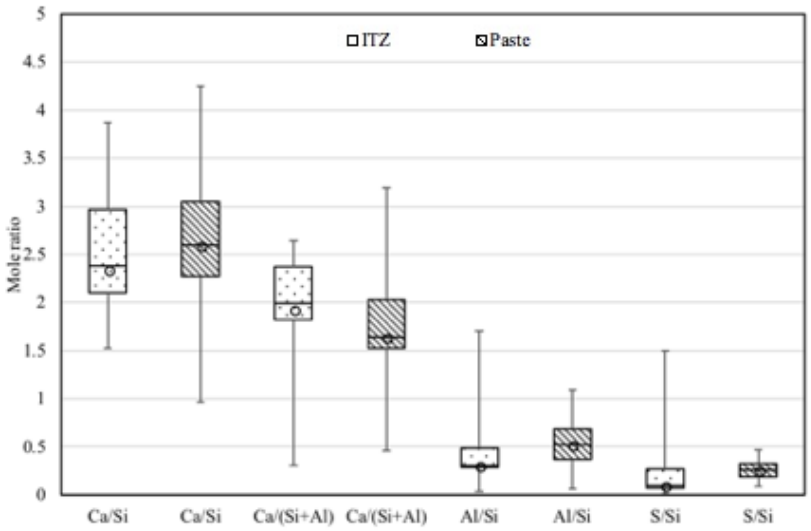


**Figure 3.18** Box plot of Ca/Si, Ca/(Si+Al), Al/Si, and S/Si mole ratio in the ITZ and paste of mixture HVFA-NS-Coat

## 3.4 Summary and Conclusions

This chapter explored the effect of using a surface treatment method to test the properties of HVFA concrete. This surface treatment method aimed at improving the ITZ of concrete by targeting the surface of coarse aggregate with nanomaterials instead of admixing nanomaterials directly during concrete mixing. By adding graphene oxide or nanosilica to cement paste that featured a lower water/cement ratio, coarse aggregate was coated with a paste film. Macroscopic properties of microstructure examination of the concrete that contained the treated coarse aggregate were investigated.

The compressive strength of the treated HVFA concrete was not increased by the surface treatment, while the splitting tensile strength was improved at the curing time of 28 days, which was comparable to that of OPC concrete. This finding can be explained by the strengthened ITZ between coarse aggregate and the paste matrix, resulting in an improved bond between them and therefore the resistance to splitting.

Mixture HVFA-NS-Coat that contained nanosilica-treated coarse aggregate performed best in the water sorptivity, chloride migration, and freezing-thawing cycle tests. All of these tests confirmed that the surface treatment of coarse aggregate by coating it with the nanosilica-containing cement paste was effective at improving the ITZ. Moreover, this approach needs a much lower dosage of nanomaterials than generally used in concrete.

Microscopic investigation shows that the microstructure of the ITZ of treated concrete improved as the porosity of ITZ decreased. The presence of more hydration products in the ITZ was also confirmed by the content change of the primary element and the elemental mole ratio obtained from the EDS data.

# CHAPTER 4 CONCLUSION

This laboratory study explored the surface treatment of fly ash particles or coarse aggregate by dip-coating nanomaterials or by aqueous nanofilm growth. The main goal was to find an approach that targets the surface of fly ash particles or coarse aggregate with nanomaterials instead of admixing them directly in the concrete matrix. By adopting this treatment, the vulnerable area in the concrete can be improved with much less nanomaterial than is usually used.

While surface treatment of fly ash particles did not result in any significant increase in the compressive strength, water sorptivity, or gas permeability of HFVA mortars that contained the treated fly ash particles, coating coarse aggregate with nanomaterial-containing cement paste showed promise as a means of improving the properties of HVFA concretes.

By adding graphene oxide or nanosilica to cement paste that featured a lower water/cement ratio, coarse aggregate was coated with a paste film. The splitting tensile strength of HVFA concretes containing treated coarse aggregate was improved at the curing time of 28 days, which was comparable to that of OPC concrete. Mixture HVFA-NS-Coat that contained nanosilica-treated coarse aggregate performed better in water sorptivity, chloride migration, and freezing-thawing cycle tests than the control mixture that contained pure cement paste-coated coarse aggregate. Microscopic investigation confirmed that the microstructure of the ITZ in treated concrete was improved. A denser microstructure and lower porosity of the ITZ in concrete that contained nanosilica-coated coarse aggregate was observed, which demonstrates the improvement in the aforementioned macroscopic properties of HVFA concretes.

## CHAPTER 5 REFERENCES


[1] Celik, K., Meral, C., Mancio, M., Mehta, P. K., and Monteiro, P. J. M. (2014). "A comparative study of self-consolidating concretes incorporating high-volume natural pozzolan or high-volume fly ash," *Constr. Build. Mater.*, 67, 14–19, Sep.

[2] Blissett, R. S., and Rowson, N. A. (2012). "A review of the multi-component utilisation of coal fly ash," *Fuel*, 97, 1–23, Jul.

[3] Wang, S. (2008). "Application of solid ash based catalysts in heterogeneous catalysis," *Environ. Sci. Technol.*, 42(19), 7055–7063, Oct.

[4] Yao, Z. T., et al. (2015). "A comprehensive review on the applications of coal fly ash," *Earth-Sci. Rev.*, 141, 105–121, Feb.

[5] Cho, H., Oh, D., and Kim, K. (2005). "A study on removal characteristics of heavy metals from aqueous solution by fly ash," *J. Hazard. Mater.*, 127(1–3), 187–195, Dec.

[6] Zhang, M. H., and Canmet (1995). "Microstructure, crack propagation, and mechanical properties of cement pastes containing high volumes of fly ashes," *Cem. Concr. Res.*, 25(6), 1165–1178, Aug.

[7] De la Varga, I., Spragg, R. P., Di Bella, C., Castro, J., Bentz, D. P., and Weiss, J. (2014). "Fluid transport in high volume fly ash mixtures with and without internal curing," *Cem. Concr. Compos.*, 45, 102–110, Jan.

[8] Malhotra, V. M. (2002). "High-Performance High-Volume Fly Ash Concrete," *Concr. Int.*, 24(7), 30–34, Jul.

[9] Malhotra, V. M. (1986). "Superplasticized fly ash concrete for structural applications," *Concr. Int.*, 8(12), 28–31, Dec.

[10] Lam, L., Wong, Y. L., and Poon, C. S. (2000). "Degree of hydration and gel/space ratio of high-volume fly ash/cement systems," *Cem. Concr. Res.*, 30(5), 747–756.

[11] Raki, L., Beaudoin, J., Alizadeh, R., Makar, J., and Sato, T. (2010). "Cement and concrete nanoscience and nanotechnology," *Materials*, 3(2), 918–942, Feb.

[12] Birgisson, B., et al. (2012). *Nanotechnology in Concrete Materials: A Synopsis*. Washington, D.C.: Transportation Research Board.

[13] Sobolev, K. (2015). "Nanotechnology and nanoengineering of construction materials," in *Nanotechnology in Construction*, Springer, Cham, pp. 3–13.

[14] Ning, X., Xianming, S., Yudong, D., and Alexandra, P. (2016). "Upcycling of waste materials: Green binder prepared with pure coal fly ash," *J. Mater. Civ. Eng.*, 28(3), p. 04015138, Mar.

[15] Feldman, R. F., Carette, G. G., and Malhotra, V. M. (1990). "Studies on mechanics of development of physical and mechanical properties of high-volume fly ash-cement pastes," *Cem. Concr. Compos.*, 12(4), 245–251.

[16] Lam, L., Wong, Y. L., and Poon, C. S. (2000). “Degree of hydration and gel/space ratio of high-volume fly ash/cement systems,” *Cem. Concr. Res.*, 30(5), 747–756.

[17] Wang, S., Baxter, L., and Fonseca, F. (2008). “Biomass fly ash in concrete: SEM, EDX and ESEM analysis,” *Fuel*, 87(3), 372–379.

[18] Bae, S., Meral, C., Oh, J., Moon, J., Kunz, M., and Monteiro, P. J. (2014). “Characterization of morphology and hydration products of high-volume fly ash paste by monochromatic scanning X-ray micro-diffraction (μ-SXRD),” *Cem. Concr. Res.*, 59, 155–164.

[19] Shi, X., Nguyen, T. A., Suo, Z., Liu, Y., and Avci, R. (2009). “Effect of nanoparticles on the anticorrosion and mechanical properties of epoxy coating,” *Surf. Coat. Technol.*, 204(3), 237–245.

[20] Li, J., Zhao, Y., Hu, J., Shu, L., and Shi, X. (2012). “Anti-icing performance of a superhydrophobic PDMS/modified nano-silica hybrid coating for insulators,” *J. Adhes. Sci. Technol.*, 26(4–5), 665–679.

[21] He, X., and Shi, X. (2008). “Chloride permeability and microstructure of Portland cement mortars incorporating nanomaterials,” *Transp. Res. Rec. J. Transp. Res. Board*, No. 2070, pp. 13–21.

[22] Han, B., Yang, Z., Shi, X., and Yu, X. (2013). “Transport properties of carbon-nanotube/cement composites,” *J. Mater. Eng. Perform.*, 22(1), 184–189.

[23] Nik, A. S., and Bahari, A. (2012). “Nano-particles in concrete and cement mixtures,” in *Applied Mechanics and Materials*, 110, 3853–3855.

[24] Norhasri, M. S. M., Hamidah, M. S., and Fadzil, A. M. (2017). “Applications of using nanomaterial in concrete: A review,” *Constr. Build. Mater.*, 133, 91–97, Feb.

[25] Han, B., Sun, S., Ding, S., Zhang, L., Yu, X., and Ou, J. (2015). “Review of nanocarbon-engineered multifunctional cementitious composites,” *Compos. Part Appl. Sci. Manuf.*, 70, 69–81, Mar.

[26] Mukhopadhyay, A. K. (2011). “Next-generation nano-based concrete construction products: a review,” *Nanotechnol. Civ. Infrastruct. Paradigm Shift*, 207–223.

[27] Shah, S. P., Hou, P., and Konsta-Gdoutos, M. S. (2016). “Nano-modification of cementitious material: toward a stronger and durable concrete,” *J. Sustain. Cem.-Based Mater.*, 5(1–2), 1–22, Mar.

[28] Aggarwal, P., Singh, R. P., and Aggarwal, Y. (2015). “Use of nano-silica in cement based materials—A review,” *Cogent Eng.*, 2(1), Aug.

[29] Sobolev, K. (2016). “Modern developments related to nanotechnology and nanoengineering of concrete,” *Front. Struct. Civ. Eng.*, 10(2), 131–141, Jun.

[30] Balaguru, P., and Chong, K. (2006). “Nanotechnology and concrete: research opportunities,” *Proc. ACI Sess. Nanotechnol. Concr. Recent Dev. Future Perspect.*

[31] Balaguru, P. N., Chong, K., and Larsen-Basse, J. (2006). “Nano-concrete: Possibilities and challenges,” in *NICOM 2: 2nd International Symposium on Nanotechnology in Construction*, 233–243.

[32] Sobolev, K., and Gutierrez, M. (2010). “How nanotechnology can change the concrete world,” *Prog. Nanotechnol. Appl.*, p. 107.

[33] Birgisson, B., Taylor, P., Armaghani, J., and Shah, S. (2010). “American road map for research for nanotechnology-based concrete materials,” *Transp. Res. Rec. J. Transp. Res. Board*, 2142, 130–137, Dec.

[34] Jennings, H. M., and Bullard, J. W. (2011). “From electrons to infrastructure: Engineering concrete from the bottom up,” *Cem. Concr. Res.*, 41(7), 727–735, Jul.

[35] Flores, I., Sobolev, K., Torres-Martinez, L., Cuellar, E., Valdez, P., and Zarazua, E. (2010). “Performance of cement systems with nano-$SiO_2$ particles produced by using the sol-gel method,” *Transp. Res. Rec. J. Transp. Res. Board*, 2141, 10–14, Dec.

[36] Muñoz, J., Meininger, R., and Youtcheff, J. (2010). “New possibilities and future pathways of nanoporous thin film technology to improve concrete performance,” *Transp. Res. Rec. J. Transp. Res. Board*, 2142, 34–41.

[37] Sanfilippo, J., Muñoz, J., Tejedor, M., Anderson, M., and Cramer, S. (2010). “Nanotechnology to manipulate the aggregate-cement paste bond effects on mortar performance,” *Transp. Res. Rec. J. Transp. Res. Board*, 2142, 29–33.

[38] Ghosh Chaudhuri, R., and Paria, S. (2011). “Core/shell nanoparticles: classes, properties, synthesis mechanisms, characterization, and applications,” *Chem. Rev.*, 112(4), 2373–2433.

[39] Yang, G., Wang, D., Yoneyama, Y., Tan, Y., and Tsubaki, N. (2012). “Facile synthesis of H-type zeolite shell on a silica substrate for tandem catalysis,” *Chem. Commun.*, 48(9), 1263–1265.

[40] Lee, M. J., et al., (2012). “Characteristics and effects of diffused water between graphene and a SiO 2 substrate,” *Nano Res.*, 5(10), 710–717.

[41] Shi, C., and Qian, J. (2000). “High performance cementing materials from industrial slags — A review,” *Resour. Conserv. Recycl.*, 29(3), 195–207, Jun.

[42] Li, W., Li, X., Chen, S. J., Liu, Y. M., Duan, W. H., and Shah, S. P. (2017). “Effects of graphene oxide on early-age hydration and electrical resistivity of Portland cement paste,” *Constr. Build. Mater.*, 136, 506–514, Apr.

[43] Ghafari, E., Costa, H., Júlio, E., Portugal, A., and Durães, L. (2014). “The effect of nanosilica addition on flowability, strength and transport properties of ultra high performance concrete,” *Mater. Des.*, 59, 1–9, Jul.

[44] Fan, Y., Zhang, S., Wang, Q., and Shah, S. P. (2015). “Effects of nano-kaolinite clay on the freeze–thaw resistance of concrete,” *Cem. Concr. Compos.*, 62, 1–12, Sep.

[45] Sato, T., and Beaudoin, J. J. (2010). “Effect of nano-CaCo3 on hydration of cement containing,” *Adv. Cem. Res.*, 23(1), 1–29.

[46] Peters, S., Rushing, T., Landis, E., and Cummins, T. (2010). “Nanocellulose and Microcellulose Fibers for Concrete,” *Transp. Res. Rec. J. Transp. Res. Board*, 2142, 25–28, Dec.

[47] Cao, Y., Zavaterri, P., Youngblood, J., Moon, R., and Weiss, J. (2015). “The influence of cellulose nanocrystal additions on the performance of cement paste,” *Cem. Concr. Compos.*, 56, 73–83, Feb.

[48] Land, G., and Stephan, D. (2015). “Preparation and application of nanoscaled C-S-H as an accelerator for cement hydration,” in *Nanotechnology in Construction*, K. Sobolev and S. P. Shah, Eds. Cham: Springer International Publishing, 117–122.

[49] Hanžič, L., and Ilić, R. (2003). “Relationship between liquid sorptivity and capillarity in concrete,” *Cem. Concr. Res.*, 33(9), 1385–1388, Sep.

[50] Han, B., Yang, Z., Shi, X., and Yu, X. (2013). “Transport properties of carbon-nanotube/cement composites,” *J. Mater. Eng. Perform.*, 22(1), 184–189, Jan.

[51] Alshamsi, A. M., and Imran, H. D. (2002). “Development of a permeability apparatus for concrete and mortar,” *Cem. Concr. Res.*, 32(6), 923–929.

[52] Spiesz, P., and Brouwers, H. J. H. (2012). “Influence of the applied voltage on the Rapid Chloride Migration (RCM) test,” *Cem. Concr. Res.*, 42(8), 1072–1082, Aug.

[53] Li, D., Chen, Y., Shen, J., Su, J., and Wu, X. (2000). “The influence of alkalinity on activation and microstructure of fly ash,” *Cem. Concr. Res.*, 30(6), 881–886.

[54] Du, S., Shi, X., and Ge, Y. (2017). “Electron probe microanalysis investigation into high-volume fly ash mortars,” *J. Mater. Civ. Eng.*, 29(7), p. 04017043.

[55] Du, S., Zhao, H., Ge, Y., Yang, Z., and Shi, X. (2017). “Laboratory investigation into the modification of transport properties of high-volume fly ash mortar by chemical admixtures,” *J. Mater. Civ. Eng.*, 29(10), p. 04017184, Oct.

[56] Zhang, Y. M., Sun, W., and Yan, H. D. (2000). “Hydration of high-volume fly ash cement pastes,” *Cem. Concr. Compos.*, 22(6), 445–452, Dec.

[57] Hou, P., Wang, K., Qian, J., Kawashima, S., Kong, D., and Shah, S. P. (2012). “Effects of colloidal nanoSiO2 on fly ash hydration,” *Cem. Concr. Compos.*, 34(10), 1095–1103, Nov.

[58] Hou, P., Kawashima, S., Wang, K., Corr, D. J., Qian, J., and Shah, S. P. (2013). “Effects of colloidal nanosilica on rheological and mechanical properties of fly ash–cement mortar,” *Cem. Concr. Compos.*, 35(1), 12–22, Jan.

[59] van der Wegen, G., Polder, R. B., and van Breugel, K. (2012). “Guideline for service life design of structural concrete: A performance based approach with regard to chloride induced corrosion,” *Heron*, 57(3), 153–168.

[60] Sanfilippo, J., Muñoz, J., Tejedor, M., Anderson, M., and Cramer, S. (2010). “Nanotechnology to manipulate the aggregate-cement paste bond effects on mortar performance,” *Transp. Res. Rec. J. Transp. Res. Board*, 2142, 29–33, Dec.

[61] Scrivener, K. L., Crumbie, A. K., and Laugesen, P. (2004). “The interfacial transition zone (ITZ) between cement paste and aggregate in concrete,” *Interface Sci.*, 12(4), 411–421.

[62] Ji, T. (2005). “Preliminary study on the water permeability and microstructure of concrete incorporating nano-SiO2,” *Cem. Concr. Res.*, 35(10), 1943–1947, Oct.

[63] Liang, Y., Ye, Z., Vernerey, F., and Xi, Y. (2015). “Development of processing methods to improve strength of concrete with 100% recycled coarse aggregate,” *J. Mater. Civ. Eng.*, 27(5), p. 04014163, May.

[64] Zhang, H., Zhao, Y., Meng, T., and Shah, S. P. (2016). “Surface treatment on recycled coarse aggregates with nanomaterials,” *J. Mater. Civ. Eng.*, 28(2), p. 04015094, Feb.

[65] Muñoz, J., Meininger, R., and Youtcheff, J. (2010). “New possibilities and future pathways of nanoporous thin film technology to improve concrete performance,” *Transp. Res. Rec. J. Transp. Res. Board*, 2142, 34–41, Dec.

[66] Moon, G. D., Oh, S., and Choi, Y. C. (2016) “Effects of the physicochemical properties of fly ash on the compressive strength of high-volume fly ash mortar,” *Constr. Build. Mater.*, 124, 1072–1080, Oct.

[67] Huang, C.-H., Lin, S.-K., Chang, C.-S., and Chen, H.-J. (2013). “Mix proportions and mechanical properties of concrete containing very high-volume of Class F fly ash,” *Constr. Build. Mater.*, 46, 71–78, Sep.

[68] Şahmaran, M., Yaman, İ. Ö., and Tokyay, M. (2009). “Transport and mechanical properties of self consolidating concrete with high volume fly ash,” *Cem. Concr. Compos.*, 31(2), 99–106, Feb.

[69] Van den Heede, P., Gruyaert, E., and De Belie, N. (2010). “Transport properties of high-volume fly ash concrete: Capillary water sorption, water sorption under vacuum and gas permeability,” *Cem. Concr. Compos.*, 32(10), 749–756, Nov.

[70] Naik, T. R., Singh, S. S., and Hossain, M. M. (1994). “Permeability of concrete containing large amounts of fly ash,” *Cem. Concr. Res.*, 24(5), 913–922.

[71] Brent Rollins, A. (2016). “Utilizing Colloidal Nano-Silica as Treatment for Concrete in Salt Water Ports: Laboratory Chloride Diffusion, Life Cycle Modeling, and the Port of Marseille Test Case,” in *Ports 2016*, pp. 736–745.

[72] Sujjavanich, S., Sida, V., and Suwanvitaya, P. (2005). “Chloride permeability and corrosion risk of high-volume fly ash concrete with mid-range water reducer,” *Mater. J.*, 102(3), 177–182, May.

[73] Bouzoubaâ, N., Zhang, M. H., and Malhotra, V. M. (2000). “Laboratory-produced high-volume fly ash blended cements: compressive strength and resistance to the chloride-ion penetration of concrete,” *Cem. Concr. Res.*, 30(7), 1037–1046, Jul.

[74] Dinakar, P., Babu, K. G., and Santhanam, M. (2008). “Durability properties of high volume fly ash self compacting concretes,” *Cem. Concr. Compos.*, 30(10), 880–886, Nov.

[75] Rossignolo, J. A. (2009). “Interfacial interactions in concretes with silica fume and SBR latex,” *Constr. Build. Mater.*, 23(2), 817–821.

[76] Bouzoubaa, N., Fournier, B., Malhotra, V. M. and Golden, D. M. (2002). “Mechanical properties and durability of concrete made with high-volume fly ash blended cement produced in cement plant,” *ACI Mater. J.*, 99(6), 560–567.

[77] Van den Heede, P., Furniere, J., and De Belie, N. (2013). “Influence of air entraining agents on deicing salt scaling resistance and transport properties of high-volume fly ash concrete,” *Cem. Concr. Compos.*, 37, 293–303, Mar.

[78] Wang, S., Llamazos, E., Baxter, L., and Fonseca, F. (2008). “Durability of biomass fly ash concrete: Freezing and thawing and rapid chloride permeability tests,” *Fuel*, 87(3), 359–364, Mar.

[79] Liu, Z., and Hansen, W. (2015). “Freezing characteristics of air-entrained concrete in the presence of deicing salt,” *Cem. Concr. Res.*, 74, 10–18, Aug.

[80] Richardson, I. G., and Groves, G. W. (1993). “Microstructure and microanalysis of hardened ordinary Portland cement pastes,” *J. Mater. Sci.*, 28(1), 265–277, Jan.